Catalogs of Hot White Dwarfs in the Milky Way from GALEX's Ultraviolet Sky Surveys. Constraining Stellar Evolution.

Luciana Bianchi[1]⋆, Boryana Efremova[1], James Herald[1], Léo Girardi[2],
Alexandre Zabot[3], Paola Marigo[4] and Christopher Martin[5]

[1] *Department of Physics and Astronomy, Johns Hopkins University, 3400 N.Charles St., Baltimore, MD 21218, USA; bianchi@pha.jhu.edu*
[2] *Astronomical Observatory of Padova, INAF, Vicolo dell'Osservatorio 5, I-35122 Padova, Italy*
[3] *Universidade Federal da Fronteira Sul, Campus de Laranjeiras do Sul, Brazil*
[4] *Dept. of Astronomy, University of Padua, Vicolo dell'Osservatorio 3, I-35122, Padova. Italy*
[5] *CA Institute of Technology, Pasadena, USA*

ABSTRACT

We present comprehensive catalogs of hot star candidates in the Milky Way, selected from GALEX far-UV (FUV, 1344-1786Å) and near-UV (NUV, 1771-2831Å) imaging. The FUV and NUV photometry allows us to extract the hottest stellar objects, in particular hot white dwarfs (WD), which are elusive at other wavelengths because of their high temperatures and faint optical luminosities. We generated catalogs of UV sources from two GALEX's surveys: AIS (All-Sky Imaging Survey, depth ABmag∼19.9/20.8 in FUV/NUV) and MIS (Medium-depth Imaging Survey, depth ∼22.6/22.7mag). The two catalogs (from GALEX fifth data release) contain 65.3/12.6 million (AIS/MIS) unique UV sources with error$_{NUV}$⩽0.5mag, over 21,435/1,579 square degrees. We also constructed subcatalogs of the UV sources with matched optical photometry from SDSS (seventh data release): these contain 0.6/0.9million (AIS/MIS) sources with errors ⩽0.3mag in both FUV and NUV, excluding sources with multiple optical counterparts, over an area of 7,325/1,103 square degrees. All catalogs are available online. We then selected 28,319 (AIS) / 9,028 (MIS) matched sources with FUV-NUV<-0.13; this color cut corresponds to stellar T_{eff} hotter than ∼18,000 K (the exact value varying with gravity). An additional color cut of NUV-r>0.1 isolates binaries with largely differing T_{eff} 's, and some intruding QSOs (more numerous at faint magnitudes). Available spectroscopy for a subsample indicates that hot-star candidates with NUV-r<0.1 (mostly "single" hot stars) have negligible contamination by non-stellar objects. We discuss the distribution of sources in the catalogs, and the effects of error and color cuts on the samples. The density of hot-star candidates increases from high to low Galactic latitudes, but drops on the MW plane due to dust extinction. Our hot-star counts at all latitudes are better matched by Milky Way models computed with an initial-final mass relation (IFMR) that favours lower final masses. The model analysis indicates that the brightest sample is likely composed of WDs located in the thin disk, at typical distances between 0.15-1kpc, while the fainter sample comprises also a fraction of thick disk and halo stars. Proper motion distributions, available only for the bright sample (NUV<18 mag), are consistent with the kinematics of a thin-disk population.

Key words: Astronomical Data Bases: catalogues — stars: white dwarfs — stars: evolution — Galaxy: stellar content — ultraviolet: stars — galaxies: Milky Way

1 INTRODUCTION

The vast majority of stars (initial mass ⩽$8M_\odot$) end their lives as white dwarfs (WD), after passing through the

⋆ E-mail: bianchi@pha.jhu.edu

asymptotic giant branch (AGB) and planetary nebula (PN) phases, in which they shed much of their mass. The ejected material enriches the interstellar medium (ISM) with newly synthesized nuclear products (mainly He, C, N, and possibly O), to different extents, depending on the initial stellar mass and exact evolutionary path (e.g. Marigo 2001, Karakas 2010). Intermediate mass stars are the main providers of carbon and nitrogen, whereas low-mass stars are the most relevant component for the mass budget of stellar remnants in galaxies. Most of the stellar mass is shed in the AGB and PN phases, but the evolution through these phases is still subject to considerable uncertainties, in particular regarding mass loss and the efficiency of the third dredge-up. Stars within an intial mass range of $\sim$0.8 to $8M_\odot$ end as WDs with a narrow mass range, mostly below $0.8M_\odot$. It is important to understand how the mass of their precursors relates to the final WD mass, in order to understand the relative contribution of different stars to the chemical enrichment of elements such as He, C, N and O.

While the evolution of the WD progenitors in the main sequence phase is fairly well understood and observationally constrained, the hot-WD population is hitherto quite elusive, owing to their small radius, hence low optical luminosity, and extremely hot temperatures, to which optical colors are insensitive (see e.g. Bianchi (2007), Bianchi et al. (2007a), Bianchi et al. (2007b)) as well as to their very short lifetimes on the constant-luminosity post-AGB phase. To make matters more difficult, the post-AGB luminosity at a given stellar temperature varies significantly according to the stellar mass, making it impossible to infer absolute luminosity from other physical parameters. The evolutionary time spent on the constant-luminosity post-AGB phase and on the cooling track is also a strong function of the mass (Vassiliadis & Woods 1994). Therefore, the exact relation between progenitor's initial mass and WD mass (initial-final mass relation, IFMR), remains to date a crucial missing link in our understanding of stellar evolution and chemical enrichment of the Galaxy.

A characterization of the population of hot WDs in the Milky Way can reduce these uncertainties, and lead to a better understanding of processes that drive the chemical evolution of galaxies like the Milky Way. UV photometry combined with optical measurements significantly increases the sensitivity to the hottest temperatures. For example, the color difference between a $T_{\rm eff}$ =50,000K and 20,000K star is about 1.5mag in FUV-g, but <0.4mag in U-B, and <0.15 mag in g-r which are comparable to photometric errors when large surveys are considered. The sensitivity gained by extending the measurements to UV wavelengths is more critical for discerning the hottest stars (see e.g. Fig.s 5-7 of Bianchi et al. (2007a) and Bianchi 2009).

The census and characterization of cool compact objects has significantly improved in recent years thanks to optical and IR surveys. The Eisenstein et al. (2006) catalog from the SDSS fourth data release (DR4) contains 9316 spectroscopically confirmed WDs and 928 subdwarfs over an area of 4783deg^2; about one fourth (2741) have $T_{\rm eff}$ >18,000K as estimated by the SDSS pipeline automated spectral analysis. An additional $\sim$5-6000 WD are expected from DR7 (Kleinman, Nitta, & Koester (2009)). Seven ultra-cool WD were added to the census by Harris et al. (2008). Gontcharov et al (2010) extracted from 2MASS, Tycho-2,

XPM and UCAC3 catalogs combined 34 WDs, 1996 evolved (11,000<$T_{\rm eff}$ <60,000K) and 7769 unevolved ($T_{\rm eff}$ <7,000K) subdwarfs, using multicolor photometry and proper motions of stars with 6<K_s<14 mag. The current version (2008) of the McCook & Sion (1999) catalog of spectroscopically confirmed WDs includes 10132 entries (all types), a factor of five increase over a decade, with respect to the original (1999) version listing 2249 WDs. Vennes et al. (2002) give a catalog of 201 DA WDs, spectroscopically confirmed from the $\sim$1,000 H-rich DA WDs discovered in the 2dF QSO redshift survey; Croom et al. (2004) 2dF catalog includes 2071 WDs over 2000 deg^2. WDs in binaries from the SDSS were catalogued and studied by several authors, see e.g. Rebassa-Mansergas et al.(2010) and references therein, Silvestri et al (2007), Heller et al. (2009, WD-M star binaries) from spectroscopy; other authors used optical-IR photometry to search for binaries among the known WDs (e.g. Tremblay & Bergeron 2007, Watcher et al. 2003). Special classes such as CVs are addressed by other works (e.g. Szkody et al. 2009 and references therein, Gaensike et al. 2009), while others studied in detail the very local population (e.g. Holberg et al (2002) discuss 122 objects within 20 pc from the Sun, which they estimate to be an 80% complete sample within this distance, and which include some double-degenerate systems).

Finding the hottest, smallest stars, however, remained a challenge prior to the GALEX UV sky surveys, which provide deep sensitivity and large area coverage. For example, 105 were found in the original EUVE whole-sky survey, with small subsequent additions obtained by combining EUVE and Rosat: see e.g. Dupuis (2002) for a review and discussion. The Rosat whole-sky survey produced 175 WD in X-rays, mostly DAs (Fleming et al. 1996, from Rosat PSPC).

Such catalogs of confirmed or candidate WDs enable the study of these objects as astrophysical probes, of stellar evolution, of MW structure, of the local neighborhood, etc. Most importantly, comprehensive catalogs enable selection of targets for follow-up spectroscopy, which then provides the detailed physics of these objects, especially when extended to the UV and far-UV wavelengths, as proven by the score of results enabled by IUE, FUSE, and HST spectrographs.

Bianchi (2009, 2007), Bianchi et al. (2009a, 2007a, 2005) have demonstrated the power of far-UV and near-UV measurements, afforded for the first time over large areas of the sky by GALEX, to unambiguously detect and characterize extremely hot stellar sources. Not only the UV wavelengths are more sensitive to the temperatures of hottest stars, but the combination of UV and optical colors allows a better separation of different classes of astrophysical objects (e.g. Bianchi 2009 and references therein).

Our present work provides a selection of hot-star candidates from UV photometry; about 40,000 hot-star candidates with FUV, NUV photometric errors⩽0.3mag (about 74,000 with photometric errors⩽0.5mag) have also SDSS optical photometry. The majority are likley hot WD with log(g) between 7 and 9. The catalog covers different latitudes and enables a first analysis of this stellar population with Milky Way models. Larger catalogs of UV sources with and without optical SDSS match are also constructed, and made available as online products.

In Section 2 we describe the method used to construct "clean" catalogs of unique UV sources from two GALEX sur-

veys with different depths and coverage, and subsets of these catalogs with matched optical photometry, and we present the catalogs' characteristics. In Section 3 we extract samples of hot-star candidates, and we analyze them with Milky Way models in Section 4. Discussion and conclusions are given in Section 5.

2 THE UV SKY SURVEYS AND THE SOURCE CATALOGS

2.1 The sky survey data

The Galaxy Evolution Explorer (GALEX) is imaging the sky in far-UV (FUV, 1344-1786Å, λ_{eff} = 1538.6Å) and near-UV (NUV, 1771-2831Å, λ_{eff} = 2315.7Å) simultaneously, with a field-of-view of 1.2° diameter and a resolution of 4.2/5.3″ [FUV/NUV] (Morrissey et al. (2007)). The images are sampled with 1.5″ pixels. Nested surveys with different depth and coverage are in progress. The widest sky coverage is provided by the All Sky Imaging Survey (AIS) and the Medium [depth] Imaging Survey (MIS), that reach typical depths of 19.9/20.8mag (FUV/NUV) and 22.6/22.7mag (FUV/NUV) respectively, in the AB magnitude system. The Nearby Galaxy Survey (NGS, Bianchi et al. 2003, Bianchi 2009, Gil de Paz et al. 2007), with over 300 fields at MIS depth, targeted nearby, hence fairly extended, galaxies, therefore it has been excluded in the present work, lest some sources from galaxies "shredded" by the pipeline intrude on our catalog. See also Bianchi (2009), Bianchi (2011), Bianchi et al (2011), Bianchi et al. (2007a), for a general discussion of the content of the UV sky surveys.

In this paper we use data from the GALEX fifth data release (GR5) AIS and MIS surveys, which include a total of 28,269 and 2,161 fields respectively. The data are taken from the MAST archive. We restrict the catalogs to sources within the central 1° diameter of the field (for good photometry and astrometry, and to exclude edge artifacts). With such restriction, and eliminating overlaps, these surveys cover a total unique area of 21,434.8 (AIS) and 1,578.6 (MIS) square degrees (Section 2.4). Section 2.2 describes the construction of the catalog of unique GALEX sources. In order to separate the UV sources by astrophysical classes, we examine in this work the portions of the GALEX GR5 AIS and MIS surveys that are also included in the footprint of the Sloan Digital Sky Survey seventh data release (DR7), which provides five optical magnitudes: $u\,g\,r\,i\,z$ in addition to the GALEX FUV, NUV magnitudes. The overlap between GALEX GR5 and SDSS DR7 includes 10,316 / 1,655 (AIS/MIS) GALEX fields, and the area coverage of the overlap is 7,325 (AIS) and 1,103 (MIS) square degrees. Details of the area calculation are provided in Section 2.4. The sky coverage of AIS and MIS in the GALEX data release GR5 and its overlap with SDSS DR7 are shown in Fig. 1.

2.2 The catalog of unique UV sources

Here we describe the procedure used to construct the catalog of unique GALEX sources (i.e. eliminating repeated measurements). All catalogs described in this paper are made publicly available from our website http://dolomiti.pha.jhu.edu/uvsky , and from MAST at

http://galex.stsci.edu , and as High-Level Science Products (http://archive.stsci.edu/hlsp/ , in the "Catalogs" section). Therefore, we provide here information on how they were constructed that will be relevant for potential users, as well as to others interested in constructing future versions of similar samples.

We extracted catalogs of GALEX sources from STScI MAST (www.mast.stsci.edu), at the CASJobs SQL interface (www.galex.stsci.edu). Sources were extracted from the table "photoobjall", from the MIS and AIS surveys separately, with the criteria that the source distance from the field center had to be ⩽0.5° and the photometric error less than 0.5 mag in NUV. In other words, we initially included in our general GALEX source catalog all NUV reliable detections, regardless of whether they have also an FUV detection. For our selection of hot star candidates, we will eventually impose the additional criterion of good FUV photometry. The additional restriction of err$_{FUV}$ <0.5 mag signifi-caly reduces the number of sources (by a factor of up to 10, see Table 2), with respect to the total number of NUV detections, and of course introduces a bias in the source catalog, the hottest and bluest sources (the subject of this paper) being not affected but the redder sources being progressively eliminated, as discussed in sections 2.5 and 3.3. For more discussions about statistical properties, and biases inherent to sample selections, see Bianchi et al (2011).

A few observations planned as part of the MIS or AIS surveys actually partly failed, and resulted in one of the detectors (most often FUV) not being exposed (such observations are typically repeated later). The observations with one of the two bands having zero exposure time were eliminated from our catalog, otherwise they will bias the statistics of FUV-detection over number of total NUV detections, and the corresponding fields were not counted in the area calculation.

Fig. 2 shows the distribution of exposure times (FUV is shown, but NUV is generally equal or larger), for the AIS and MIS fields. The typical exposure time for MIS is 1500 sec, which is met or exceeded by the majority of fields. The AIS survey aims at exposure times of the order of ∼100 sec. We retained also fields with exposures shorter than typical. Therefore, while the typical depth of the two surveys (AIS and MIS) differ by ∼2 mag, the exposure level is not strictly homogeneous across each catalog.

Fig. 2-bottom panel shows the number of GALEX sources in each GALEX field. We color-coded the fields by three ranges of exposure time for the AIS (two for MIS), since the number of sources detected above a given error-cut generally increases with exposure time. This plot is useful to check for fields with overdensities, since the surveys, the broad AIS in particular, include also some stellar clusters. In general the spread in number of sources per field is just about a factor of two for MIS. A few AIS fields around latitude -30° have an overdensity of almost one dex, however the total number of AIS fields in each 10°-wide latitude bin (used in our analysis, see next section) is very large, and a few overdensities do not affect our analysis of stellar counts with Milky Way models over wide areas. Fields with high density of sources, and in particular the stellar clusters included in the surveys, will be separately analyzed elsewhere. They are included in our catalog for completeness and for
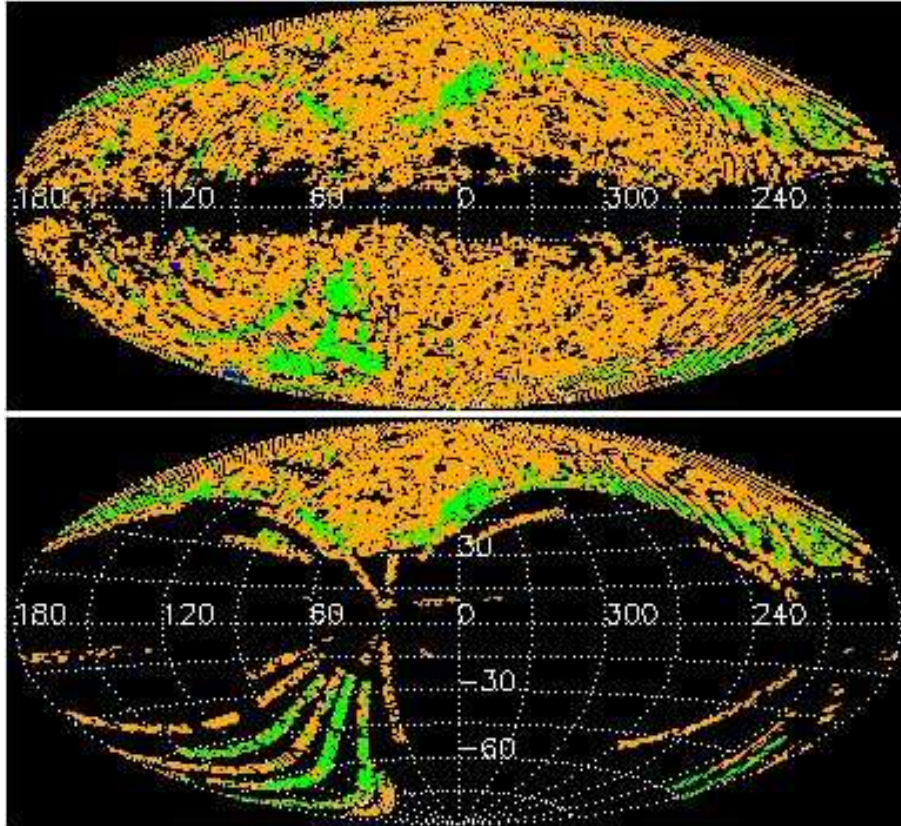
Figure 1. TOP: Sky coverage (in Galactic coordinates) of the GALEX data release GR5 showing the major surveys: AIS (orange), MIS (green), DIS (blue). BOTTOM: the portion of the GALEX GR5 sky coverage for AIS and MIS overlapping with SDSS seventh data realease (DR7)

possible use by others, although customized photometry is desirable in very crowded fields (e.g. de Martino et al. 2008).

Nearby galaxies are generally observed as part of the 'NGS' survey which is excluded from our catalog, but a few large galaxies are also in the footprint of AIS and MIS and bright knots of galaxies "shredded" by the pipeline may enter the catalog as separate sources (see Bianchi et al. (2007a)). A few such sources may have FUV-NUV<-0.13 and appear pointlike in the SDSS catalog, and therefore may enter our catalog of hot-star candidates (section 3), but they would not affect the statistical results. For other, more specific uses of our catalog, they may be removed by checking against a list of nearby galaxies, as we did in Bianchi et al. (2007a). Using the "child" flags from the SDSS pipeline, that track deblended sources, proved not to be useful in indentifying and weeding out sources from "shredded galaxies".

The searches and download of GALEX sources with the above criteria were done using the java CASJobs command-line tool (casjobs.jar). One problem we often encountered when using this tool to extract and download query results from the database is that sometimes the download pipe gets broken prematurely, and the results are truncated without any warning being given. In order to verify that the output file contained all the results, a separate count query was run on the SQL server and compared to the number of output sources in the downloaded file each time. It was necessary to subdivide the search in small latitude strips due to various limits set by the CASjobs interface (e.g. query length, output

file size), as well as to avoid the frequent problem of the long searches being interrupted.

The GALEX archive contains multiple observations of the same source, when some fields overlap or are repeated. Having all measurements of each source is useful for variability studies (which will be addressed in a forthcoming work), and for chosing the best measurement when several are available. For our present purpose we constructed from the total output a unique-source catalog, in the following manner. GALEX sources were considered possible duplicates if they lied within 2.5$''$ of each other. If two GALEX sources were within this distance, but had the same "photoextrac-tid" (i.e., they are both from the same observation) they were both considered unique. Otherwise, they were assumed to be multiple observations of the same source. We choose, to represent the unique source, the measurement with the longest NUV exposure time. In the case of equal exposure times, the observation where the source was closer to the field center was chosen (i.e. the source with the smallest "fov_radius" value from the "photoobjall" table), as photometric quality is usually better in the central part of the field.

2.3 The matched UV-optical source catalog

A portion of the GALEX survey areas is in the footprint of the SDSS DR7 (see Fig.1 - bottom panel), and for the UV sources in this area we constructed a catalog of matched
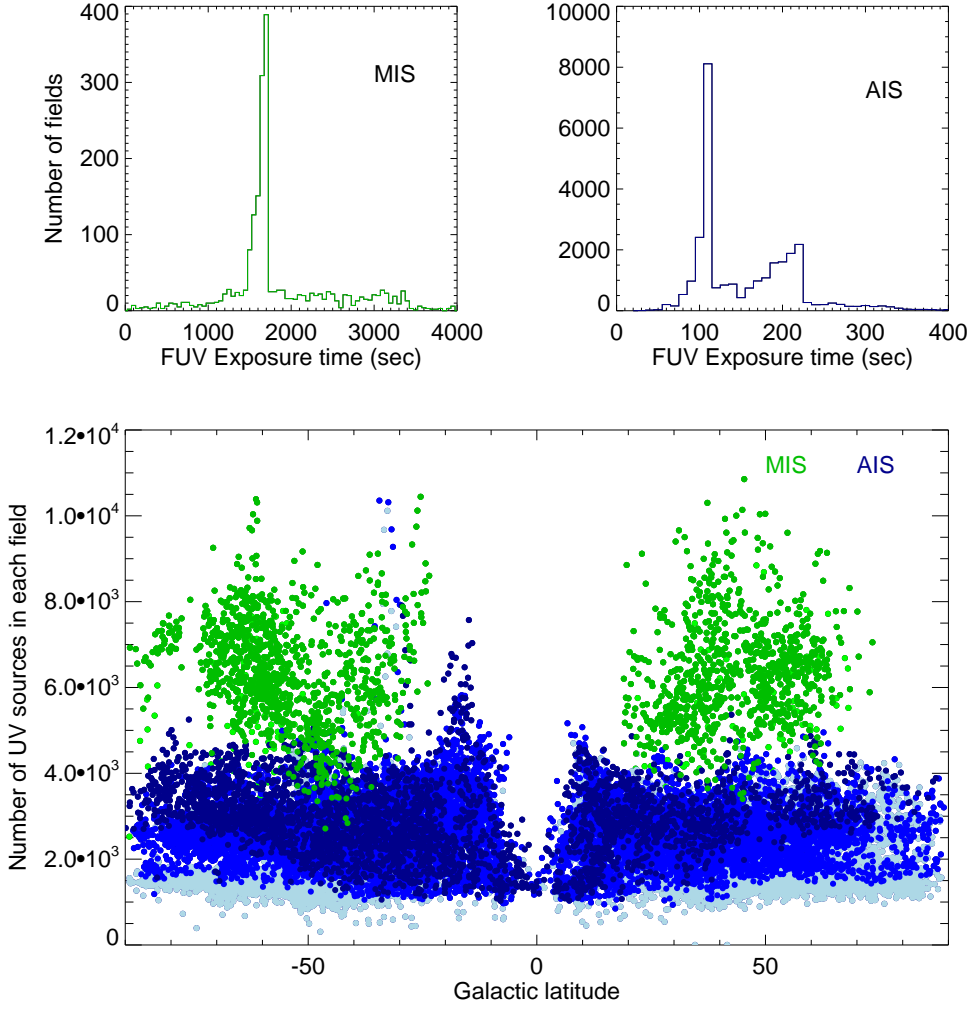
Figure 2. TOP: distribution of FUV exposure times for AIS (10sec bins) and MIS surveys (50sec bins); a few fields have longer exposure times, off the scale of the plots.   BOTTOM: Number of UV sources (all UV detections, not just our selected hot stars) in each GALEX field (1° diameter), before merging the catalogs and removing overlaps. Three shades of blue (light/medium/dark) for AIS indicate exposure times of <120 / 120-220 / >220 sec respectively, and lighter / darker green for MIS fields indicate FUV exposures less/more than 1200 sec. Generally the number of UV source detections in a field increases with depth of exposure, as expected, and as seen more distinctly for the AIS at the high latitudes, uncomplicated by dust extinction. A few fields, including some with short exposures, have overdensities. While the number of MW stars increases towards the MW disk, as shown by the AIS sources, at MIS depth most UV sources are extragalactic, hence show no correlation with Galactic latitude except for the foreground extinction. The sharp drop in the center, due to dust extinction, defines the MW dust disk.

optical sources. We uploaded the coordinates of our GALEX unique sources into the SDSS SQL interface (version 3_5_16 rev 1.70, at casjobs.sdss.org) and queried for SDSS matches against the "photoprimary" table (SDSS source catalog that includes only unique sources) using an inital search radius of $4.2''$. A match radius of $3''$ was eventually used in the final catalog, as we shall see.

As with the GALEX searches, the SDSS searches were done in an automated way on 1°-wide Galactic latitude strips using the casjobs command-line tool. We found that there is currently a bug in the SDSS version of this tool (v0.03) that causes the last character of a file to be dropped when extracting query results. We compensated for this by

writing our query to pad the end of the file with an additional character.

2.3.1 Multiple matches.

A given GALEX source may have multiple SDSS matches within the search radius, given the higher spatial resolution of the SDSS ($\sim 1.4''$). In such cases the CASjob search returns multiple lines with the same GALEX source and the various SDSS matches. We "ranked" the multiple SDSS matched sources based on the distance, with the closest SDSS source being retained as the "match" for the GALEX source and the additional SDSS sources being noted. When using UV-optical colors for source classification, UV sources
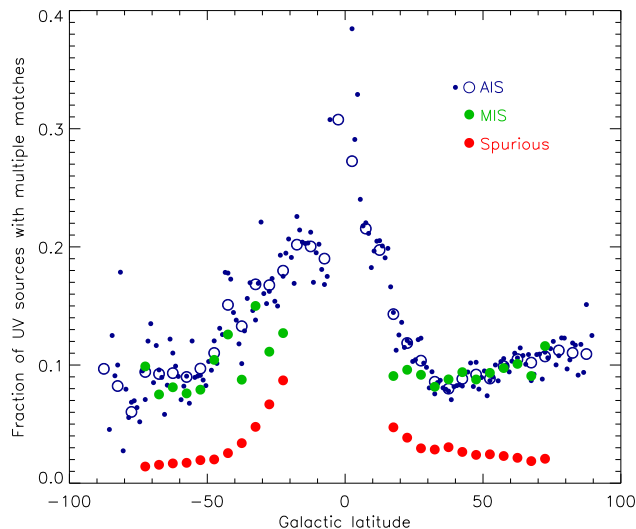
Figure 3. Fraction of UV sources having multiple optical matches within a $3''$ match radius, as a function of Galactic latitude. Green dots show MIS data, blue dots show AIS data, divided in strips of $1°$ (small dots), as well as averaged over $5°$ (blue circles). The increase towards the Galactic plane reflects the higher density of optical sources at low MW latitudes. The plot also shows a slight North-South asymmetry. The fractions shown are for point-like sources, with error cuts of 0.3 mag. The fraction increases if a larger match radius is used. The red dots are the incidence of spurious matches (see text).

with multiple optical matches must be excluded, because, even though the closest optical source may be the actual counterpart, the UV photometry at the GALEX spatial resolution of $\sim 5''$ may be a composite measure of two optical sources, and therefore the color would not be meaningful. The fraction of UV sources with multiple optical matches, eliminated from the analysis sample, is then taken into account when estimating density of astrophysical sources (# per square degree). This fraction is given in Table 2. Sources with multiple optical matches are listed separately in our hot-star catalogs, and are included with "rank">0 in the total matched-source catalog. The relative number of UV sources with multiple optical matches, shown in Figure 3, increases towards low Galactic latitudes, as expected. The figure refers to our final catalog with match radius of $3''$, and pointlike sources only: approximately 10% of the UV sources have more than one optical counterpart, at intermediate and high Galactic latitudes, in agreement with our previous work on earlier data releases which covered mainly high Galactic latitudes (Bianchi et al. 2005, 2007a). The fraction increases to slightly over 20% for latitudes $|b| \approx 10\text{-}20°$, reflecting the higher density of stars in the MW disk, and is still very uncertain at latitudes $|b| < 10°$, where we have little area coverage. For a larger match radius ($4.2''$), the fraction of multiple matches increases significantly, relative to the total number of matches, and so does the incidence of spurious matches (Sect. 2.3.3), therefore we adopted a final match radius of $3''$ in our catalog. The fraction is also higher if exended sources are included.

2.3.2 Other caveats.

In the interest of others who may want to apply the same procedures, we also mention that, due to the large current area coverage and consequent large number of sources, when it is necessary to perform the searches on small contiguous portions of the sky (e.g. $1°$ strips), it may happen that the coordinates of a GALEX UV source fall in one strip (close to the latitude limit), and the SDSS match falls in the next latitude range, due to a small difference in coordinates. Such cases are included in the final catalogs in the latitude range which is appropriate according to the position of the GALEX source. Care should also be taken when using the Galactic coordinates as returned by the GALEX database, as those coordinates differ by $\lesssim 0.5''$ from those derived by converting the GALEX RA, Dec coordinates to Galactic coordinates using standard astronomical packages (e.g., WCSTools from the Smithsonian Astrophysical Observatory). These differences probably arise because the GALEX database stores Galactic coordinates using real data types, while using double precision data types to store RA and Dec values. Therefore, sorting GALEX search results based on the Galactic coordinates returned by the database may give different results than using WCSTools to derive those coordinates from the GALEX RA and Dec.

Another contingency that must be tested for, in the above procedures, is whether a given SDSS source matches multiple GALEX sources. This can occur if a SDSS source lies somewhere in between two GALEX sources which were deemed unique. In this case, the match query returns a match of each of the GALEX sources with the same SDSS object. We retain the match with the GALEX source which is the closest to the SDSS source, and eliminate the other. This occurs rarely.

2.3.3 Spurious matches.

The probability of spurious matches was estimated as follows. We randomly selected 30% of the coordinates from our matched GALEX-SDSS catalogs (in separate $5°$ bins of Galatic latitude), and searched the SDSS database against coordinates offset by $0.5'$ from those of the real sources. The spurious match rate, shown in Fig. 3 (red dots), is the number of incidences where one or more matches were found (within a search radius of 3") divided by the number of uploaded coordinates. As for the multiple matches, it is higher towards the Galactic plane, where the stellar density increases and therefore also the probability of random matches within a given radius. The rate is of the order of a few% at high and intermediate latitudes. However, matches that are positional coincidences are likely to have odd colors and the fraction may be lower in selected analysis samples.

2.3.4 Comparison with other catalogs

We point out, in the interest of users of our catalogs, that there are several differences from other basic matched source catalogs posted on MAST. Most notably, we include only the central $1°$ diameter portion of the field, therefore we conservatively eliminate all edge sources (mostly defects or bad measurements but also some good sources), but we retain

all good portions. Second, we consider all existing measurements for each source, from which the best is chosen. For example, the matched catalog described by Budavari et al. (2009) instead, eliminates overlap by reducing each GALEX field to an hexagon (selection of primary). In this procedure, the vertices of the hexagons include sources near the edge (i.e. possibly also sources with poor photometry, and artifacts). Moreover, since the hexagons are fixed at nominal positions, but the actual pointings may differ, unnecessary gaps between fields (which may not exist in the actual observations) are introduced, as the authors point out. Our partition, described in section 2.4, and following Bianchi et al. (2007b), avoids such problems and enables better and more homogeneous photometry quality, as well as easy and precise calculations of the unique-area coverage for our GALEX surveys, and of overlap area with any other survey, consistent with the actual source catalog rather than with nominal field centers. This is preferable for our analysis. Such differences may cause samples selected from different matched catalogs, to differ slightly.

2.4 Area coverage

In order to derive the density of sources extracted from our catalogs, we computed the total areas of unique coverage, taking into account overlap between fields, in the GALEX GR5, and then the area overlapping with SDSS DR7, following the method of Bianchi et al. (2007b). Since we restricted the catalogs to sources within the central $1°$ of the GALEX field, for each field we considered an effective radius of $0.5°$. Our code scans the entire sky and calculates the unique area covered by the GALEX fields, and the portion of this area covered also by the SDSS. First, the whole sky is divided in small, approximately square, tassels, along Galactic longitude and latitude. We used steps in l,b of $0.05/0.1°$ for MIS/AIS respectively. Then, we find the distance between the center of each tassel in our whole-sky grid and the center of each GALEX field, and sum the areas of the tassels that are within half degree of a field center, avoiding to count the same tassel twice, which eliminates overlap between fields.

The error in the estimated area depends on the step used to calculate the grid of tassels (tassel size), and the number of tassels. The area of each tassel decreases at high latitudes (the step in l,b is kept constant over the whole sky), hence the statistical error due to the tassels along the field's edge (i.e. tassels that fall partly inside and partly outside the $1°$ circle of a GALEX field) varies with the location of the fields, both with latitude and with the relative location of the field center to a grid step. Such errors cancel out statistically for a large number of fields. For a very small area however, i.e. for a few fields, it is desirable to use smaller tassels. We estimate the uncertainty by computing the areas several times, each time offsetting the positions of the GALEX field centers by about half the size of a tassel, in both latitude and longitude directions. The resulting uncertainty is $\lesssim 1$ square degree, for our total area and the areas of each latitude bin.

In order to calculate the area of overlap between the GALEX MIS and AIS surveys and SDSS DR7, we initially matched the centers of all tassels included in our GALEX coverage (MIS and AIS) to the SDSS DR7 footprint: the areas of tassels deemed within the SDSS footprint were summed to obtain the area coverage of our matched

source catalogs. However, we discovered an issue in the SDSS database DR7 footprint that prevented its use for calculating the overlap areas. The output returned from the SDSS database footprint query is currently somewhat incorrect, perhaps due to some SDSS fields which appear included in the DR7 footprint in the database (therefore counting towards area coverage in any estimate), however do not have sources in the "photoprimary" table or corresponding images because the observation failed or was marked as bad for some reason. We have consulted several experts of the SDSS database, but we found no way so far to identify such fields specifically. When we plotted on the sky the SDSS matched sources (obtained from the SDSS "photoprimary" catalog), and the sky-tassels deemed by the footprint-query to be within the footprint, we noted some not irrelevant areas of mismatch (most notably, in the latitude strip 50-60°South we found the largest "false positive" area, about $17.5 \deg^2$ in total; the discrepancies are much smaller at other latitudes). We attempted to perform the footprint query on the SDSS database using different syntaxes. Specifically, a basic all-inclusive footprint SQL search returns several "false-positive" answers (i.e. several contiguous areas that the database considers within the footprint, have no SDSS sources), hence the area based on such outputs would be overestimated with respect to the source catalog; a more detailed footprint query, confining the search to "PRIMARY" footprint area, returns both false-positives and false-negatives. We finally could not use the SDSS footprint query, and wrote a separate code to independently search, for our entire GALEX sky coverage, sub-areas with and without SDSS sources; we considered the areas devoided of any SDSS sources as outside the SDSS footprint[1]. This procedure was complicated because (1) in order to decide whether a tassel contained SDSS sources, we had to consider SDSS sources of any color, not just our hot-star catalog (which includes the rarest stars in the sky, hence some tassels may actually not have any hot star even though they are located within the footprint), and (2) we had to consider much larger sky-tassels than our original grid, to avoid false-negatives, and then iterate within the "positive" tassels with a progressively finer grid (down to $0.05\deg^2$, about 1/16th of a GALEX field), to confine the uncertainty of the area estimate. It is important for our analysis, which compares density of sources (#/square degree) with model predictions, to estimate areas *consistent* with the source catalog used, in this case the PRIMARY catalog from the SDSS. We used our area estimates in the following analysis. We stress, for future reference, that there was no way to detect the inconsistency between catalog and database footprint other than by plotting the distribution of sources and footprint-tassels on sky coordinates in various ways. This is a desirable test on any such work.

The GALEX GR5 AIS and MIS sky coverage, and the GALEX-SDSS overlap area in the matched GR5xDR7 releases, restricting the GALEX field to $1°$ diameter and eliminating overlaps between GALEX fields, are given in Table

---

[1] These regions may be 'in' the footprint for SDSS database purposes, but they contribute no sources to the catalog, hence counting them towards the area coverage would be inconsistent

1, for the whole coverage and for separate ranges of Galactic latitude.

2.5 Catalog statistics and effect of error cuts on the sample

Figure 4 shows the UV magnitude distribution of our GALEX unique-source catalog, and the effect of progressive error cuts in NUV, and in both NUV and FUV. While a progressively stringent error cut in one band (NUV) simply truncates the sample to a brighter magnitude limit, an additional error cut in FUV, which effectively raises the faint limit of the sample in this band, causes a relatively higher decrease of redder sources, and the histogram of sources distribution becomes double-peaked. The same effects are seen (right panel) for the matched GALEX-SDSS sources catalog. This catalog can also be separated in pointlike and extended sources using the SDSS spatial information ($\sim 1.4''$ resolution). Such distinction shows that most of the faint-magnitude peak of the source distribution is due to extended sources, which are likely galaxies, as can be expected (e.g. Bianchi 2009). The most restricted sample in the right-panel histograms, the point-like matched sources with error $\leqslant 0.3$mag in both FUV and NUV, and FUV-NUV<-0.13, is the subject of this paper; it contains mostly hot star candidates ($T_{\rm eff} >$ approximately 18000K), with some contamination by QSOs at faint magnitudes and red optical colors, discussed in section 3.2 (see also Bianchi et al. (2009a)).

The analysis of the hot-star sample with Milky Way models (see later) shows that the magnitude limit introduced by our error cut of $\leqslant 0.3$ mag eliminates mostly halo and thick-disk MW stars from the sample (between the green solid- and dashed-lines on the right-hand panel). On the other hand, including sources with larger photometric errors would introduce significant contamination of the sample by non-stellar objects (see Fig 5).

More statistical analysis of the catalogs, and discussion of potential biases in flux-limited sample selection, are given by Bianchi et al (2011).

3   SELECTION OF HOT STARS

The matched GALEX-SDSS sources in our catalogs are shown in color-color diagrams in Figure 5 as density plots. Model colors for major classes of astrophysical objects are also shown to guide the eye in interpreting the distribution of sources. We refer to Bianchi et al. (2009a) and references therein for other similar figures and description of the model colors.

We selected hot stellar candidates by extracting the matched pointlike sources with FUV-NUV < -0.13 (in the AB magnitude system), which corresponds to stars hotter than $\approx$18,000 K, the precise $T_{\rm eff}$ depending on the stellar gravity, and on the model atmospheres adopted (discussed later).[2] This FUV-NUV limit was chosen to largely exclude

all extragalactic objects, based on colors derived from canonical templates of QSOs and galaxies (e.g. Bianchi 2009 and references therein, see also Fig. 5).

As shown by Figure 5 in this work, and by Fig. 7 (lower panels) Bianchi et al. (2007a), at AIS depth ($\sim$21th mag) sources with FUV-NUV < -0.13 have very little contamination by extragalactic objects, but at fainter magnitudes a number of QSOs and galaxies with extremely "blue" FUV-NUV colors is found. Bianchi et al. (2009a) have examined the nature of such uncommon QSOs, and their Figure 1 and 2 show the location of these objects in the color-color diagrams. These QSOs have extremely "blue" FUV-NUV (more negative than typical QSOs at any redshift), but optical colors typical of QSOs and galaxies. Therefore they overlap, in UV–optical color-color diagrams, with the locus of hot stars with a cool companion, i.e. hot stars having very blue (i.e. negative) FUV-NUV color but optical colors redder than what their FUV-NUV would imply for a single hot source. We discuss the QSO contamination in section 3.2.

We restricted the catalog to sources with photometric errors $\leqslant 0.3$mag in both FUV and NUV. Fig. 4, previously discussed, and Table 2 in this work show the effect of the error cuts on the sample's statistics. We additionally use one optical band (r) to separate the hot sources in "single" star candidates, having color NUV-r<0.1, and "binary" candidates having NUV-r>0.1. In more detail, the NUV-r boundary between single and binary hot stars has a complex dependence on stellar $T_{\rm eff}$ and radii of the binary pair, which we will address in a different work. For example, a hot WD with an A-type companion, and pairs with small mass ratios will fall in the color selection of our "single" hot-star sample. The adopted value is a useful cut to eliminate most extragalactic sources contaminating our FUV-NUV<-0.13 sample, as they have NUV-r>0.1, however it is obviously an oversimplification for a detailed study of binaries. In sum, our so-called (for simplicity) "binary" sample includes stellar pairs with a hot WD and a cooler star, and some QSOs; the "single" sample includes all single stars and some binaries. We impose no error cut on the r magnitudes, in order to not limit the sample of the hottest WDs, which are faint at optical wavelengths. If the restriction of error$\leqslant 0.3$ mag were imposed to the r-band, the density of objects in the MIS sample would be reduced by about 30% (GALEX is 'deeper' than SDSS for very hot stars of low luminosity, see section 3.1); the loss would be much smaller for the brighter AIS sample.

The density of hot-star candidates is shown in Fig. 6 and will be discussed later. The magnitude distribution of the total hot-star candidate sample (FUV-NUV < -0.13) is shown with shadowed histograms in Figures 8 and beyond, and the "single" hot star candidates (FUV-NUV < -0.13 and NUV-r<0.1) with solid-color histograms.

---

[2] The measured colors also depend on extinction, however for a Milky Way-type dust, with R_V=3.1, and moderate reddening amounts, the GALEX FUV-NUV color is basically reddening-

free. In fact, the higher selective extinction A_λ / E_{B-V} in the FUV range is approximately equalled by the effect of the broad 2175Å feature in the NUV range, see Fig. 2, and Bianchi (2009). The absorption in each UV band, however, is much higher than in optical bands.
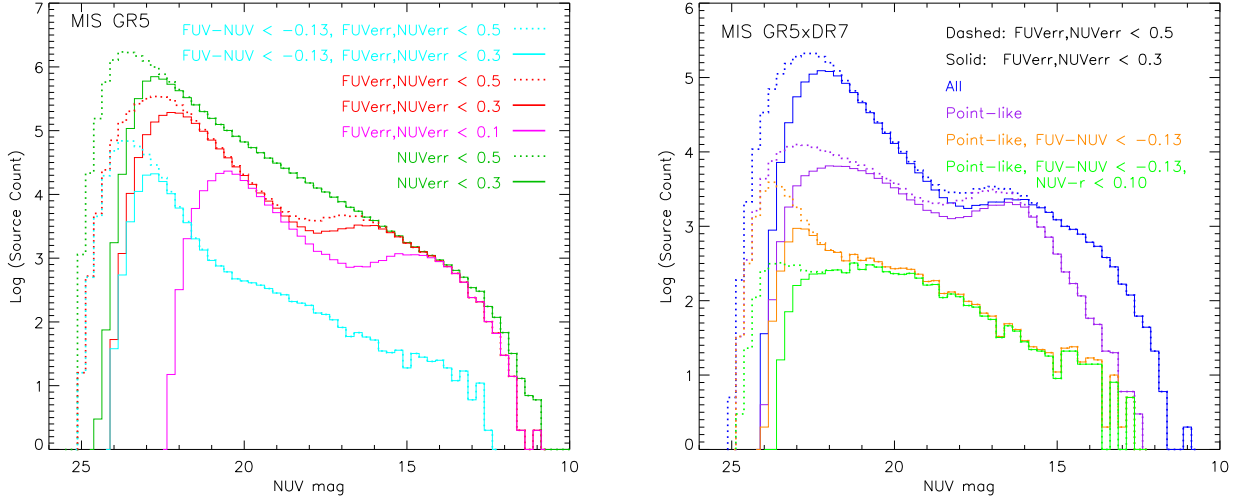
Figure 4. Distribution of UV sources in NUV magnitudes, and effects of error cuts and color cuts. **LEFT**: the whole catalog of GALEX unique sources (MIS), described in Section 2.2, with progressive error cuts in NUV, and in both FUV and NUV. A more stringent NUV error cut simply causes a brighter cutoff at the faint end, as expected, while the requirement of significant detection (or good photometry) also in FUV modifies the overall distribution ("redder" sources being eliminated), which becomes double-peaked. The distribution of the "bluest" sources (FUV-NUV <-0.13), which include hot stars (this paper) and some QSOs (Bianchi et al. 2009a) is also shown. **RIGHT**: NUV magnitude distribution of the matched UV-optical sources. Here we also use the spatial information from the optical data, to separate point-sources (eliminating most galaxies, but not QSOs with a high contrast between the central source and the underlying galaxy). The point-like sources with FUV-NUV<-0.13 and FUV, NUV error ⩽0.3mag (solid orange line) are the hot star candidate sample analyzed in this paper, and the green histogram are the "single" hot stars. The figure, with the analysis in section 4, shows that a potential halo component (NUV~24-25mag) is eliminated by our error cut at the current survey's depth; on the other hand, including objects with larger errors would cause our color selection to include low z QSOs.
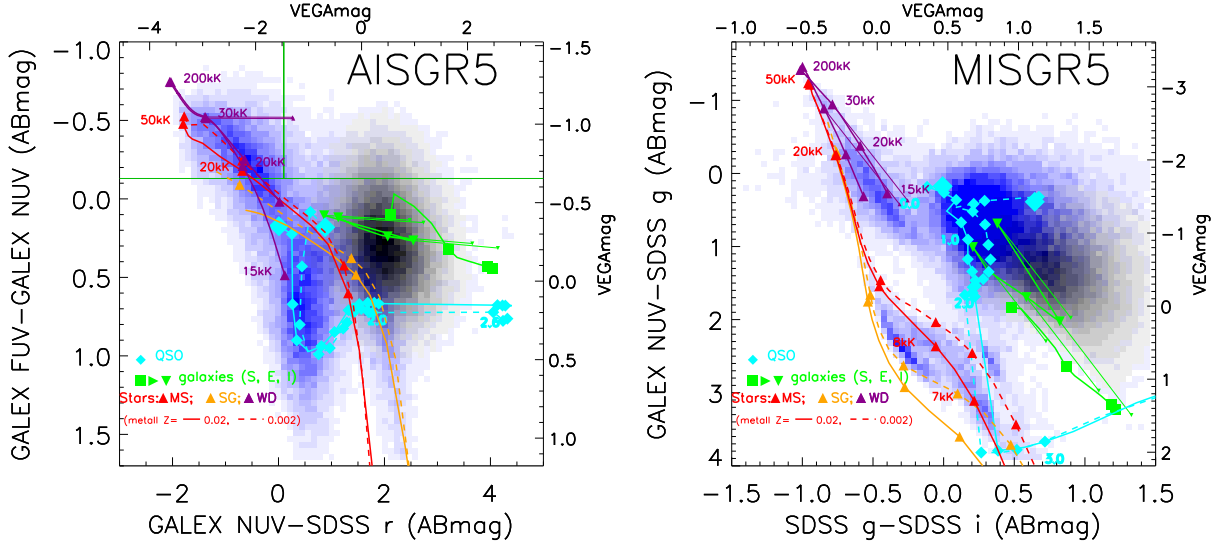
Figure 5. Color-color diagrams for the GALEX UV sources matched to SDSS sources, at AIS and MIS depth. Blue/black densities are pointlike/extended sources respectively. Model colors for stars (T$_{eff}$ sequence, for different gravities), QSO (redshift sequence, cyan) and galaxies (age sequences, green) are shown. The two purple stellar sequences (label "WD") in the right-side panel are for logg=9.0 and 7.0. Although gravity cannot be separated well photometrically at high T_{eff} 's, the vast majority of hot stellar sources are clustered in between these two model sequences, and much fewer are seen along the logg=5 and 3 (red and yellow) sequences at hot temperatures, as expected. In the ≈ 2.5mag shallower AIS survey the relative number of stars and extragalactic objects is comparable, while at MIS depth the latter dominate. From such diagrams the hot star samples are selected (see text), with color cuts shown by the green lines in the left-hand plot.

3.1 Hot Stars not detected by SDSS

While the SDSS depth of 22.3/23.3/23.1/22.3/20.8 AB mag in u,g,r,i,z provides a fairly complete match to the AIS UV source catalog, the hottest, smallest stars detected in the MIS may fall below the SDSS limit. This can be guessed by comparing in Fig.s 8, 10, 12 the green-dashed histogram (matched GALEX-SDSS sources with FUV-NUV<-0.13) with the light-green filled-color histogram (matched sources with FUV-NUV<-0.13 and NUV-r<0.1, i.e. "single" hot stars). The hottest single WDs will be faintest at optical wavelengths (e.g. a star with log g=9. and $T_{\rm eff}$ =50,000/100,000 K would have FUV-r=-2.33/-2.61 in AB mag, according to our TLUSTY model grids). Therefore, hot WDs still detectable in UV at the depth of our MIS sample (see Fig. 4) may be below the SDSS detection limit, while hot WDs with an optically-brighter binary companion or QSOs, which have redder UV-optical colors, will be detectable also in the SDSS imaging. This explains why the density of MIS "single" hot matched sources (light-green) drops at faint magnitudes earlier than the dashed-green histogram, the difference between the two being larger than what can be ascribed to QSO contamination (Section 3.2).

In order to estimate the incompletess of faint hot-WD counts in our matched sample, we searched for GALEX MIS sources with FUV-NUV<-0.13 that are within the SDSS DR7 footprint, but do not have SDSS counterpart. We found ≈1,500 such sources, having no optical match in our catalog with a match radius of $3''$ (section 2.3). We performed a number of tests to verify if these are real sources. We matched them against the SDSS catalog, extending the match radius to $6''$, and found 399 additional matches, 138 of them are classified as "pointlike" sources at the sdss resolution. These mostly appear to be actual sources in the images, although we note that for faint sources, the SDSS classification of "extended" and "pointlike" is not always reliable, as shown by Bianchi et al. (2009a). It is expected that a small number of sources may have optical coordinates differing by more than $3''$ from the UV position; sometimes this is due to a nearby source not fully resolved. For the remaining 1,100 UV sources with no SDSS match out to $6''$, visual inspection of random subsamples revealed some to be part of extended cirrus emission, many seem likely sources, a few cases are parts of a shredded galaxy. The 'kron radius' from the GALEX pipeline gives an indication of the spatial extent of the source: 189 sources have kron radius larger than 3.5, hence are probably not stellar sources, but visual inspection suggests about 75% of them to be real sources. Even visual inspection however is not always conclusive, for faint sources or complicated fields, and better resolution or deeper exposures would be needed for a final sample. In sum, a very large fraction of the 1,500 objects unmatched within $3''$ are actual sources, and an undetermined fraction may be actual hot stars.

In spite of the large uncertainties, we added all these objects to the "single" hot matched sources catalog, and show the total as filled-dark-green histograms in Fig.s 6, 8, 10, 12. They must be considered a very generous upper limit, and only a reminder that the light-green histograms suffer from incompleteness for hot stars with NUV fainter than ∼22mag.

3.2 Purity and completeness of the sample

In order to estimate the probability that the photometrically-selected hot star candidates actually are hot stars, and the possible contamination of the sample by other types of objects, we examined the subsamples of our catalogs for which SDSS spectra exist. Out of 9,028 MIS matched sources with FUV-NUV<-0.13 and FUV,NUV error ⩽0.3mag, 810 have SDSS spectra, 104 of which are sources with NUV-r>0.1, i.e. in the "binaries" *locus*. Of these "binary" candidates with existing spectra, 58 are spectroscopically classified by the SDSS pipeline as stars, 4 as galaxies, 42 as QSOs. Therefore, almost half of the MIS sources with FUV-NUV<-0.13 and NUV-r>0.1 could be QSOs (as found also by Bianchi et al. (2007a)), and half could be hot stars with a cool companion. In more detail, QSOs numbers increase at fainter magnitudes, and have FUV-NUV colors closer to our limit (-0.13) than the hot WD (Bianchi et al. (2009a)). Because stars and QSO counts vary with magnitude in different ways, and especially because this statistic can be highly biased by the SDSS selection of spectroscopic targets, which is of course unrelated to our present selection, and because the spectroscopic survey does not reach the depth of the MIS photometric survey, we refrain from assuming a correction for the fraction of extragalactic objects in the binaries sample based on current data.

A much higher purity is found for the "single" hot-star candidates (FUV-NUV<-0.13 and NUV-r<0.1). Out of 4,924 in the MIS sample, 706 have spectra, 703 of which are classified as stars, and two as galaxies. Only one is classified as QSO by the SDSS spectroscopic pipeline, but it is actually a hot WD, as shown by Bianchi et al. (2009a). This implies a purity of almost 100% for the "single" hot-star candidates, down to the magnitude limit of the SDSS spectroscopy at least. Again we stress however that the spectroscopic subset is serendipitous for our purpose, but not necessarily unbiased.

In the AIS sample, out of 28,319 total hot-star candidates (21,606 of which with NUV-r<0.1), 4448 (3737) have spectra, classified as 4075 (3721) stars, 309 (9) QSOs, and 59 (7) galaxies; corresponding to 91.6% (99.6% for "single" hot-star candidates) purity. The higher content of stellar sources in the AIS sample, even for the "binaries", is due to the brighter magnitude limit.

A crude, more direct indication that there is contamination by extragalactic sources in the "binary" hot-star *locus*, is that the fraction of "binaries" (NUV-r>0.1) among the hot sources is about 25% for the AIS and 45% for the MIS. We note that the AIS value of 25% is not reflecting the fraction of actual binaries, because the pairs whose components have similar $T_{\rm eff}$ are included in the "single" color cut, and on the other hand, AIS "binaries" may also contain QSOs.

In view of the contamination by QSOs in the "binary" hot-star sample, in the following analysis with Milky Way models we will consider the counts of "single" hot-star candidates, and assume a canonical binary fraction of 30% in the models.
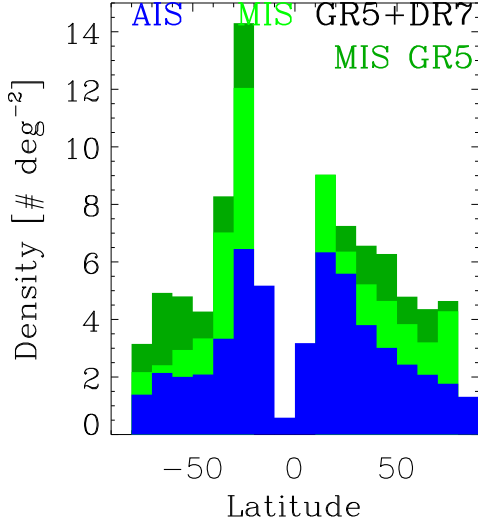
Figure 6. Density of "single" hot stars at different Galactic latitudes (all magnitudes combined, green for MIS, blue for AIS). The stellar counts are not corrected for Milky Way extinction, which is more severe at low latitudes, and causes the sharp drop seen on the MW plane. The bright-green histogram is the GALEX-SDSS matched MIS single hot-star candidates, the dark-green histogram includes also hot UV sources with no optical match, within the SDSS footprint (see text). The ranges 10-20° N and 70-80° N have only 6 and 3 square degree MIS coverage in the matched footprint, therefore the statistical significance is much less than in other bins.

3.3 Characteristics of the Hot-Star Candidate Catalog

The number of hot sources selected (pointlike, with error $\leqslant$0.3mag in FUV and NUV, and FUV-NUV<-0.13; see sect.3), and of the subset with NUV-r<0.1 ("single"), are given in the last two columns of Table 2. Stellar counts as a function of magnitude will be analyzed in the following sections. Figure 6 shows the density of "single" hot-star candidates (all magnitudes combined) as a function of Galactic latitude. The density increases by over a factor of seven, from the poles towards the Galactic plane. Owing to the MW extinction, the counts are a lower limit at all latitudes, but especially near the Galactic disk. Therefore, the variation with latitude shown by this figure is less than the actual one. For the MIS, the density of hot stars in the matched sample (light-green histogram) is incomplete due to the SDSS limit (section 3.1). The dark-green histogram shows the MIS "single" hot-star candidates including the hot GALEX sources without optical match. Sources with NUV-r>0.1 are not shown due to the QSO contamination (section 4.3); adding the stellar binaries in this color range would increase the number density but not change the trend.

In the next section we analyze the density of hot stellar candidates as a function of magnitude; the samples are divided in strips of 10° Galactic latitude, in order to examine the structure of this MW stellar component.

4 ANALYSIS. COMPARISON WITH MILKY WAY MODELS

From the point of view of stellar evolution, the sample presented in this paper includes essentially two kinds of evolved stellar objects: the post-AGB stars that have just expelled their envelopes and are crossing the HR diagram towards higher $T_{\rm eff}$'s at constant luminosity, on their way to become planetary nebule nuclei, and the hot white dwarfs which are fading both in $T_{\rm eff}$ and luminosity. Post-AGB stars are very elusive because they evolve very fast, on time-scales of the order of 10^3-10^5 years (Vassiliadis & Wood (1994)). Hot white dwarfs evolve with longer timescales, but at significantly fainter luminosities. Both are elusive at all wavelengths except the UV. Our hot-star census based on the UV sky surveys provides the first opportunity to examine a comprehensive, unbiased sample of such objects. Our hot post-AGB and WD candidate sample extends over a significant sky coverage, and clearly presents a disk-like distribution, concentrated towards the Galactic disk (Fig. 6). Such sample will be analyzed in the context of a model for the Milky Way geometry below.

4.1 Constraining Milky Way models

In this section we analyze the number counts and sky distribution of our hot star candidates, using the TRILEGAL stellar population synthesis code (Girardi et al. 2005). TRILEGAL creates mock catalogues of stars belonging to the Milky Way, and then distributes them along the line-of-sight. It extracts the simulated stars from extended libraries of evolutionary tracks and synthetic stellar spectra, assuming reasonable prescriptions for the distributions of ages, masses and metallicities of the Milky Way stellar components: thin and thick disks, halo and bulge. We note here that the bulge component does not contribute almost any source to our hot star sample, and is therefore not shown in the plots of our model results.

The thin disk density, $\rho_{\rm thin}$, decreases exponentially with the galactocentric radius, R, and as a squared hyperbolic secant function in the direction perpendicular to the plane, z:

$$\rho_{\rm disk} = C \exp(-R/h_R) \operatorname{sech}^2(2\,z/h_z)\,. \tag{1}$$

The scale length is set to $h_R = 2800$ pc, whereas the scale heigth increases with the population age t as

$$h_z(t) = 95\,(1 + t/(4.4{\rm Gyr}))^{1.67}\,, \tag{2}$$

Such an increase is necessary to describe the observed increase of the velocity dispersion W with age (see e.g. Holmberg et al. (2009)).

The thick disk follows the same functional form but with both scale parameters fixed as $h_R = 2800$ pc and $h_z = 800$ pc. The constants C, for the thin and thick disks, are adjusted so that the surface thin disk density is equal to 59 $M_\odot\,{\rm pc}^{-2}$, whereas the local thick disk density is of 0.0015 $M_\odot\,{\rm pc}^{-3}$. The halo is modeled as an oblate spheroid following a deprojected $r^{1/4}$ law, with a local density of 0.00015 $M_\odot\,{\rm pc}^{-3}$. Finally, the Sun is located at $R = 8700$ pc, $z = 24.2$ pc.

The default parameters for the geometry of the MW components in TRILEGAL are calibrated to reproduce the

star counts in a local sample extracted from the Hipparcos catalogue, and in several multiband catalogues including the shallow, all-sky 2MASS, and a few deep surveys such as EIS-deep and DMS (Girardi et al. (2005)). For regions out of the Galactic plane, i.e. for $|b| > 10°$, errors in the star counts predicted by TRILEGAL are typically of about 10 to 20% down to $K \sim 14$ (Girardi et al., in preparation).

The reddening is taken into account in the Milky Way models as follows. Along a given line-of-sight, the value of $E(B-V)$ at infinity is taken from the Schlegel et al. (1998) maps. The total extinction is then distributed along the line-of-sight as if it were generated by an exponential dust layer with scale height h_z^{dust}; its default value is $h_z^{\mathrm{dust}} = 110$ pc. In this way, the closest simulated stars are unreddened, whereas those at distances of a few hundred parsecs are reddened by the full amount predicted by the Schlegel et al. (1998) maps.

We use a new version of TRILEGAL, which has been modified for the purposes of this analysis in several ways; most of these modifications will be detailed in a subsequent paper (Zabot et al., in preparation). Post-AGB stars, planetary nebulae nuclei and white dwarfs of types DA and DB have been included using the evolutionary tracks from Vassiliadis & Wood (1994) and Althaus et al. (2001, 2005), together with the Koester (2008) synthetic spectra. In the present version we have considered only the DAs, since they are the dominant type among hot WDs (Hansen & Liebert 2003). The fraction of DBs is known to increase significantly for WDs cooler than 12000 K, thanks to convection in the He layers (Bergeron et al. 1997; Hansen & Liebert 2003). Such cool WDs, however, are not included in our selection of sources. The TRILEGAL code uses the Koester (2008) grids to assign magnitudes to the theoretical stars. In Figure 7 we show a comparison with magnitudes calculated from TLUSTY models, and in Figure 8 we compare stellar counts obatined by selecting model stars by T_{eff} and by synthetic colors, in order to illustrate the sometimes neglected effect of the model-atmosphere uncertainties.

Following our preliminary findings of discrepancies between predictions and hot star counts based on earlier data releases (Bianchi et al. 2009b), the TRILEGAL code has been modified to also allow the choice of initial–final mass relation (IMFR) independent from the prescription adopted for the previous evolutionary phases. In this way, the mass distribution of the white dwarfs does not need to follow the constraints imposed by the previous TP-AGB tracks, which come from Marigo & Girardi (2007).

Model predictions for sample Galactic latitudes are shown in Figure 8, computed with default TRILEGAL parameters for the MW geometry and the default initial-final mass relation (IMFR) from Marigo & Girardi (2007, hereafter MG07), as well as the Weidemann (2000) IFMR (hereafter W2000). We show the thin disk, thick disk, and halo stellar components, as well as the total predicted counts. The IFMR from MG07 alrgely overpredicts faint star counts, while the W2000 IFMR produces an overall better match with the observed counts, at all Galactic latitudes (see also Fig. 10), and was therefore adopted in all our calculations that follow. Given the relevance of the IFMR in the context of stellar evolution, we explain in the next section how it affects the hot-star count predictions, which can be tested by our data.
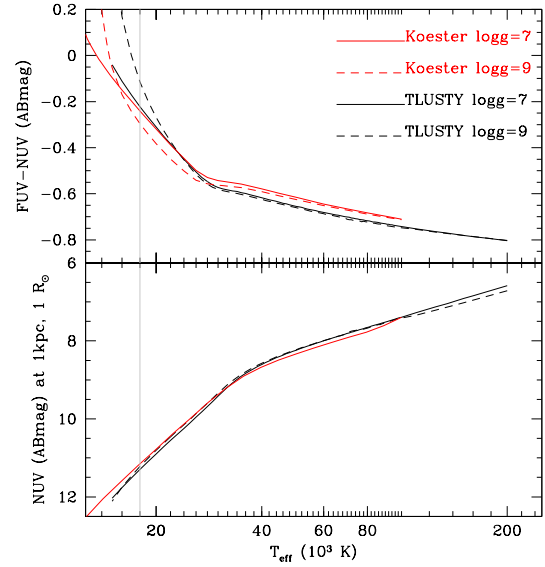

Figure 7. Comparison of model magnitudes (NUV) and color (FUV-NUV) of stars with log(g)=7.0 and 9.0, of varying T_{eff} . Model magnitudes are constructed from our grid of pure-H TLUSTY NLTE model spectra and from Koester (2008) LTE models. The latter include convection, which TLUSTY (ver198) does not. Our color cut of FUV-NUV<-0.13 corresponds to $T_{\mathrm{eff}} \approx$ 18,800/17,200K (log(g)=9.0/7.0) in the TLUSTY models, and to T_{eff} =18,000K in solar Kurucz-model colors with log(g)=5.0 (not shown). While TLUSTY and Koester model colors with log(g)=7.0 agree quite well for T_{eff} up to 26,000K, the two grids are discrepant by ~ 0.15mag for log(g)=9.0, where the Lyα wings are broad enough to enter the GALEX FUV band when convection is taken into account. The situation reverses at hotter T_{eff} 's. A color cut at FUV-NUV<-0.5 benefits from less scatter among model grids, which we could take as a measure of less uncertainty, however the resulting sample (the very hottest stars) would be drastically reduced, and so the statistical significance.

4.2   The Initial-Final Mass Relation

While the Milky Way geometry has been derived by previous studies of low mass stars, the IMFR is one of the least constrained factors in our understanding of stellar evolution, in spite of its importance for determining the yield of chemical elements, and ultimately the Galaxy chemical evolution. The reasons for this uncertainty include insufficient statistics of post-AGB stars. The final WD mass is confined to a very small range (~ 0.5-$1.0 M_\odot$) compared to the ~ 0.8-$8 M_\odot$ range of their main sequence initial masses, and the post-AGB evolutionary time-scale varies steeply within the small WD mass range. The luminosity remains constant over a large range of T_{eff} (up to >100,000K), and again depends on the remnant mass, making it much harder to establish their distance and absolute luminosity than for main sequence stars.

Therefore, the mismatch between model predictions computed with TRILEGAL's default parameters and observed stellar counts (Figure 8, top-left panel), also previously noted by Bianchi et al. (2009b), prompted us to explore different initial-final mass relations in TRILEGAL. Although other factors, such as the WD birthrate, or the assumed MW extinction model, or a different geometry may
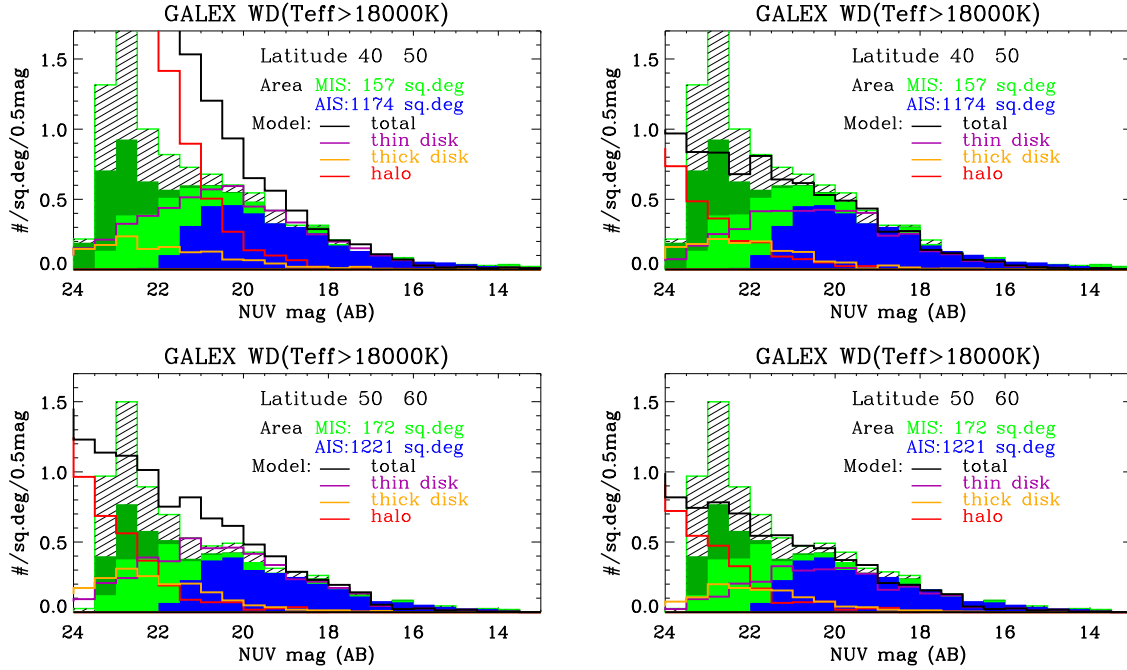
Figure 8. Modeling WD counts: the effect of the IFMR. The density of hot star candidates at two sample latitudes (10°-wide strips) are shown, with model predictions (halo, thin and thick disk components, and total) The models in the top-left panel are computed with the TRILEGAL default IFMR (MG07) and the others with W2000 IFMR. The thick disk and halo counts become significant at magnitudes fainter than ~19, and ~20, for these two IFMR respectively. Models with W2000 IFMR match better the data down to magnitudes ~20-21, below which the AIS becomes incomplete. In the top and bottom-right panels the model counts are obtained selecting stars with $T_{\rm eff}$ >18000 K in the model calculations, and in the bottom-left panel selecting stars by color cut (FUV-NUV<-0.13) with TRILEGAL's transformation from $T_{\rm eff}$ to magnitudes, from the same calculations. The comparison illustrates the uncertainties introduced by the transformation of the isochrones into magnitudes via model atmospheres. The filled-green histograms are GALEX MIS hot "single" sources with SDSS match (light green), and including sources with no SDSS detection (dark green).
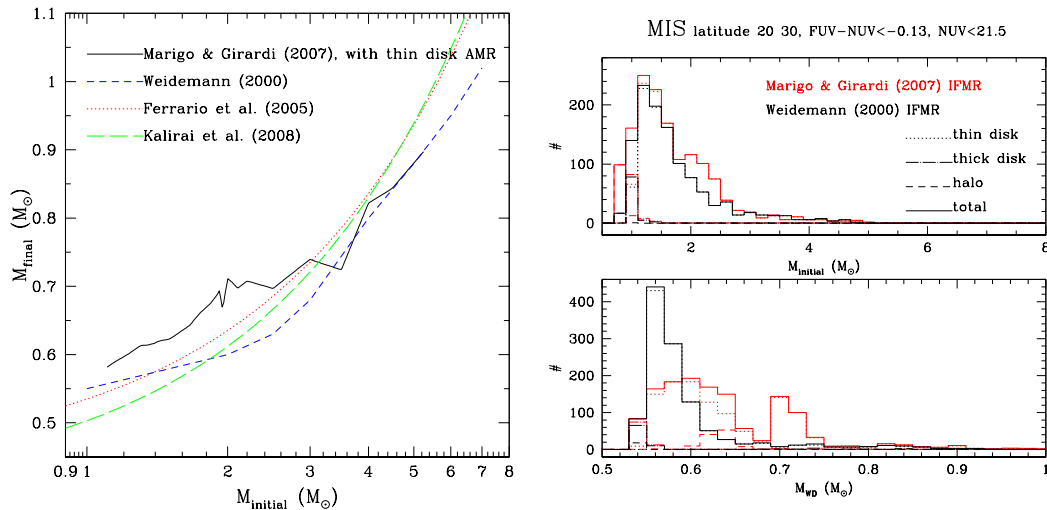
Figure 9. LEFT: Some of the IFMRs implemented in TRILEGAL, and tested in this work. The MG07 IFMR depends on metallicity, so that different age–metallicity relations (AMR) will sample it in different ways; the curve shown here is for the Rocha-Pinto et al. (2000) AMR, which is used to model the MW thin disk in TRILEGAL. Other IFMRs are the semi-empirical one from Weidemann (2000), and the purely empirical ones by Ferrario et al. (2005) and Kalirai et al. (2008). **RIGHT:** The distribution of initial and final WD masses (top and bottom panels, respectively) derived from TRILEGAL models using the Marigo & Girardi (2007, red lines) and Weidemann (2000, black lines) IFMR. The different lines illustrate the contributions from the different MW components, for one sample latitude, down to NUV= 21.5.
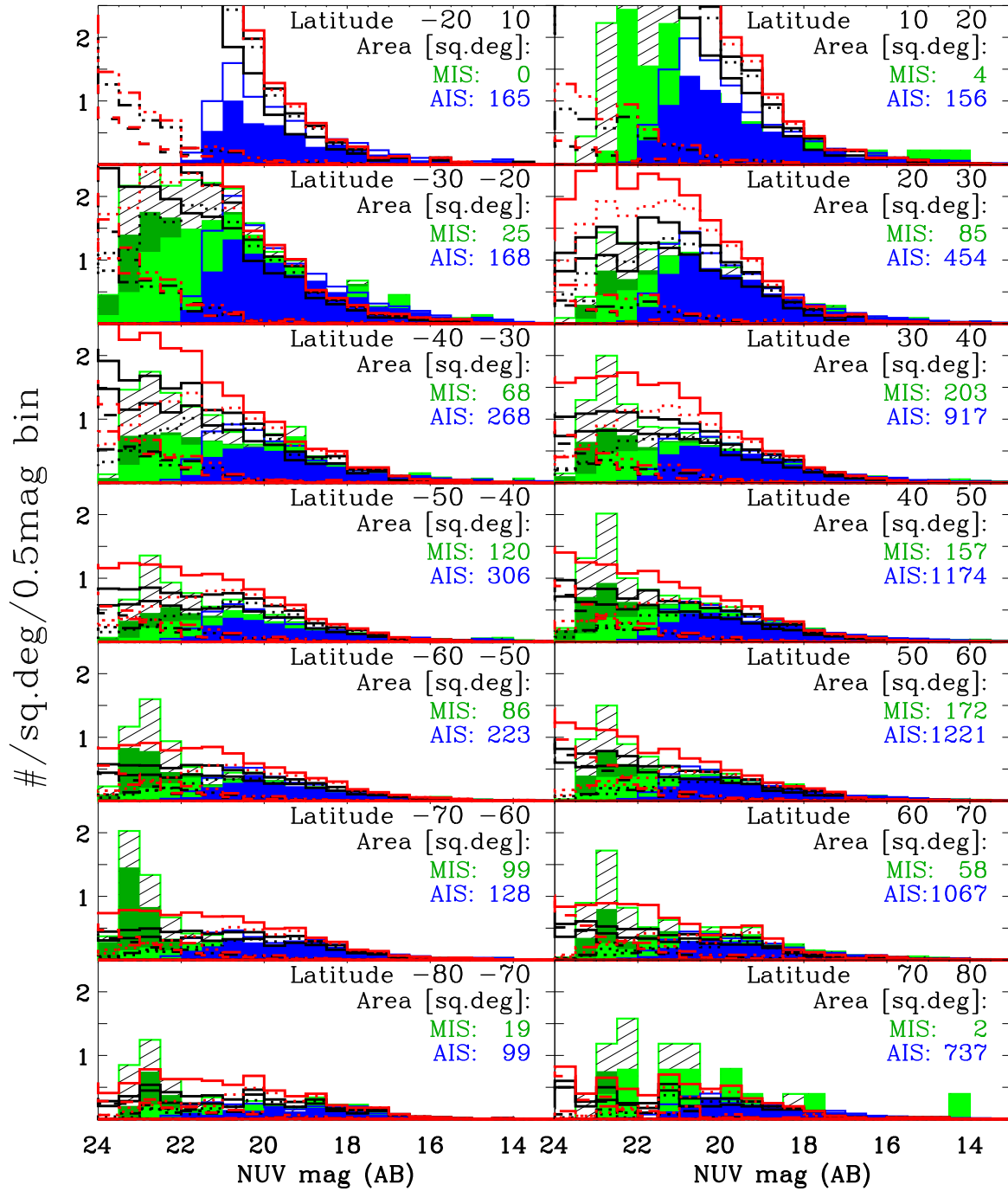
Figure 10. Density of hot stars, separated in 10° ranges of Galactic latitude. The area coverage for AIS and MIS, indicated on each panel, varies significantly among latitudes, and the statstics is better where the coverage is large. TRILEGAL model counts, computed with W2000 IFMR, are shown with lines for thin disk (dotted), thick disk (dash-dotted) and halo (dashed), as well as total (solid line). The black lines are model stars selected by $T_{eff} > 18000K$ (upper line: total, lower line: single model stars); the red lines are stars selected from the same models by color cut (FUV-NUV<-0.13) as explained in Fig.8. The match is good overall, at bright magnitudes, but better at Northern high latitudes and Southern low latitudes (except for $|b|<20°$). The dashed green-outlined histograms include both single and binary MIS hot-star candidates (the latter including also QSOs at faint magnitudes). The solid-color histograms are the "single" hot-star candidates (NUV-r<0.1). The models were computed covering the centers of the GALEX MIS fields in each latitude strip, except for the lowest latitudes ($|b|<20$) where the TRILEGAL models are computed following the distribution of the AIS fields, because MIS has little or no coverage. The large difference between North and South 20-30° latitudes, seen both in observations and predictions, is due to the MIS-SDSS overlap including more directions towards the Galactic center in the South, and away from it in the North; the longitude dependence is illustrated in Figure 11.

also affect model predictions, the IFMR is a most critical aspect for modeling hot-WD counts, and was therefore explored in this first analysis. The geometry is better constrained by low-mass stars (e.g. Girardi et al. 2005), which are more numerous, and their counts based on optical-IR bands are less affected by extinction than a UV-based catalog. The right-hand panels of Fig. 8 show that the W2000 IFMR produces a better match of the model calculations with the observed stellar counts than the MG07 IFMR, and this trend is seen at all Galactic latitudes.

These two IFMRs are illustrated in Fig. 9, together with additional IFMRs recently derived by Ferrario et al. (2005) and Kalirai et al. (2008) from extensive high-S/N spectroscopy of white dwarfs in Galactic open clusters. Despite the uncertainties related to the age-dating of the clusters, their field contamination, and the possible dependences on metallicity, they are somewhat similar to the Weidemann (2000) semi-empirical IFMR. The MG07 IFMR, instead, is derived from theoretical evolutionary tracks and, as shown in the figure, yields significantly higher final masses for all $M_{\mathrm{ini}} < 2 M_\odot$.

In order to understand why the model-predicted hot-WD counts depend on the IFMR, let us first consider the distribution of WD masses in present-day surveys of the Solar neighborhood. Empirical determinations have always concluded that the WD mass distribution presents a strong peak at low masses, with a maximum close to 0.55 or 0.65 $M_\odot$ and a well-defined tail of more massive WDs, as well as a faint low-mass tail believed to be either observational errors or the result of binary evolution (e.g. Bergeron et al. (1992); Bragaglia et al. (1995); Madej et al. (2004); Liebert et al. (2005); Kepler et al. (2007); Hu et al. (2007); Holberg et al. (2008)) .

The origin of this peaked mass distribution can be readily derived from basic population synthesis theory (see Marigo 2001; Ferrario et al. 2005). Given a volume-limited sample containing stellar populations of all ages between $T = 0$ and $T = 10$ Gyr, the distribution of WD initial masses will be given by

$$N(M_{\mathrm{ini}}) \propto \phi_M(M_{\mathrm{ini}})\, \psi[T - \tau_{\mathrm{H}}(M_{\mathrm{ini}})]\, \tau_{\mathrm{WD}}(M_{\mathrm{ini}}), \qquad (3)$$

where ϕ_M is the IMF, $\psi[T - \tau_{\mathrm{H}}]$ is the star formation rate at the time of stellar birth $T - \tau_{\mathrm{H}}$, and τ_{H} and τ_{WD} are the main sequence and WD lifetimes, respectively. The first 2 terms in the right-hand side of this equation represent the production rate (or, alternatively, the "death rate") of evolved stars with different masses, in number of stars per unit time. Considering a Salpeter (1955) IMF, $\phi_M \propto M_{\mathrm{ini}}^{-2.35}$, and a reasonably-constant star formation rate ψ over the galaxy history, the equation above indicates a marked peak of the production rate at the minimum initial mass for the formation of a white dwarf, which is about 1 $M_\odot$ for a galaxy age of $T = 10$ Gyr. For higher initial masses, the production rate should fall as $M_{\mathrm{ini}}^{-2.35}$. This behaviour will be shared by any galaxy model with nearly-constant star formation, independently of its IFMR.

Assuming a constant and monotonic IFMR, $M_{\mathrm{WD}}(M_{\mathrm{ini}})$, the WD mass distribution is given by

$$N(M_{\mathrm{WD}}) \propto \left(\frac{\mathrm{d}M_{\mathrm{WD}}}{\mathrm{d}M_{\mathrm{ini}}}\right)^{-1} N(M_{\mathrm{ini}}). \qquad (4)$$

therefore, for almost-linear and linear IFMRs like the Weide-
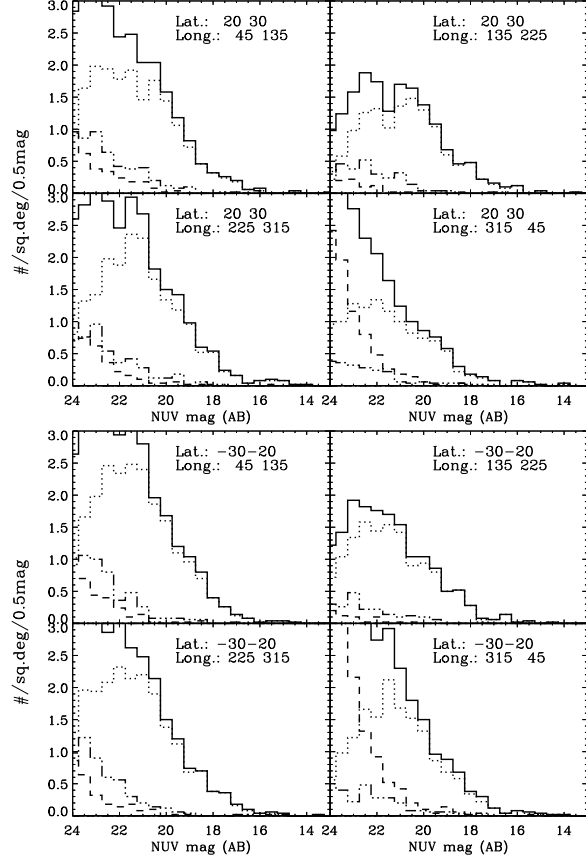
Figure 11. Model-predicted counts at latitudes between 20-30° North, and South, for four symmetric longitude quadrants. Model calculations were performed in 1° fields evenly distributed in longitude, and combined in 90° sections, to illustrate the dependence of the model-predicted hot stars counts on longitude. The strongest differences are seen between center and anti-center directions, as expected, and the North-South asymmetry is most prominent in directions towards the Galactic center. Lines show thin disk (dotted), thick disk (dash-dotted), halo (dashed) and total counts (solid).

mann (2000), Ferrario et al. (2005), and Kalirai et al. (2008) ones, the WD production rate is still expected to behave like a power-law peaked at the smallest masses. This smallest mass corresponds to a WD mass of ~ 0.55 $M_\odot$ (see Fig. 9).

The WD lifetime τ_{WD18k}, defined as the total time after the AGB in which the star will be hotter than 18,000K, is longer for WDs of higher mass, because, although they evolve much faster in the constant-luminosity phase, they reach higher T_{eff} than lower-mass WDs, and spend a longer time in their WD cooling track before fading below the Teff=18000K limit. Models using different IFMRs simply associate the final masses, hence also these τ_{WD18k} lifetimes, to different initial masses, without affecting the WD production rate. The end result in terms of mass distribution $N(M_{\mathrm{ini}})$ (see equation 4) is that smaller WD masses will weigh the distribution towards shorter τ_{WD}, hence decreasing the numbers of observed WDs with $T_{\mathrm{eff}} > 18000$K. This effect explains the higher number of hot WDs predicted by the MG07 IFMR respect to the W2000 IFMR (Fig. 8). In fact, as can be inferred from Fig. 9, the W2000 IFMR gives

Figure 12. Thin disk description. In view of the fact that our present data is most sensitive to the thin disk population, we compare model results computed with three different thin disk geometries: in the top panel the TRILEGAL default geometry, in th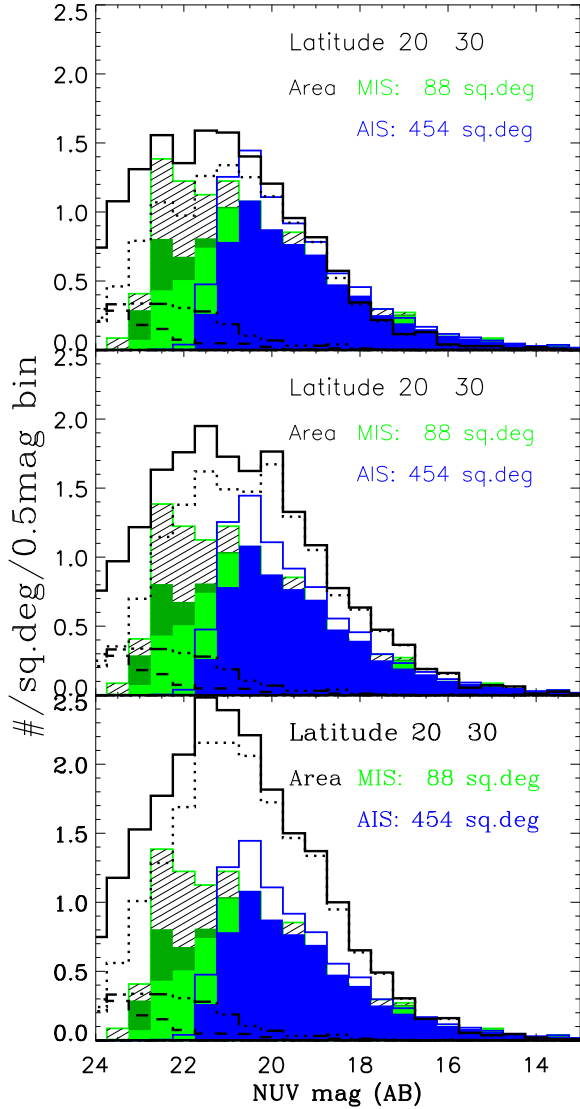e middle panel an exponential (option 1), and in the bottom panel a z sech (option 2) description (see text). The top panel, with the default geometry description given in eq. 1 and 2, gives the closest results to the observed counts, confirming previous findings by Girardi et al. (2005). This option was adopted in all our model calculations shown. Colors and symbols as in Fig. 10.

significantly lower WD final masses (hence shorter τ_{WD18k}) for the interval of initial masses between 0.6 and $\sim 2\ M_\odot$. Because of the IFM being skewed towards lower masses, these objects represent numerically the majority within the whole mass range.

Figure 9 (right panel) shows the distribution of initial and final WD masses derived from TRILEGAL for a sample latitude, using either the MG07 or W2000 IFMR. It shows that most of the hot WDs observed by GALEX are expected to derive from low-mass stars, with initial masses below $\sim$

$2\ M_\odot$. Moreover, it indicates that the bulk of observed WDs have low masses, typically $0.55 \lesssim M_{\mathrm{WD}} \lesssim 0.6\ M_\odot$ in the case of the W2000 IFMR. There is no direct confirmation of this particular prediction, although it is in line with WD mass determinations derived from spectroscopic surveys of more limited samples (e.g. Bergeron et al. 1992; Bragaglia et al. 1995; Madej et al. 2004; Liebert et al. 2005; Kepler et al. 2007; Hu et al. 2007; Holberg et al. 2008).

In the calculations with MG07 IFMR the distribution of predicted WD masses is quite different from the Weidemann (2000) case, with a broad mass distribution extending from 0.55 to 0.65 $M_\odot$, followed by a sort of gap, and a second peak of WD masses located slightly above 0.7 $M_\odot$. These features reflect the positive slope of this IFMR up to $M_{\mathrm{ini}} \lesssim 2\ M_\odot$, and its plateau at $M_{\mathrm{WD}} \simeq 0.7\ M_\odot$ for $2 \lesssim M_{\mathrm{ini}} \lesssim 3.5\ M_\odot$ (see Fig. 9 -left). Another particularity of this IFMR is the high masses (about 0.64 $M_\odot$) predicted for the WDs belonging to the halo and thick disk. This prediction conflicts with recent mass determinations of WDs in old star clusters, which indicate values close to 0.53 $M_\odot$ (Kalirai et al. 2008, 2009). A similar trend is seen at different latitudes.

Overall, an IFMR such as that of W2000 produces predicted counts closer to the observed numbers, at bright magnitudes where our sample is complete, and at the same time mass distributions in agreement with those derived from spectroscopy of nearby WDs. These aspects underscore the difficulties of deriving the IFMR from theoretical evolutionary tracks of AGB stars, even when these tracks are directly calibrated with observations of AGB stars in the Local Group, as is the case of MG07. This work, and future analyses planned on a wider sky area to explore concurrently the effects of the MW dust geometry, suggests that a deeper investigation of AGB evolution is necessary, especially concerning the theoretical prescriptions for mass loss, to reconcile constraints provided by WDs in our Galaxy and those provided by AGB stars in nearby galaxies.

We finally note that even models calculated with W2000 IFMR tend to predict more faint-star counts than our "single" WD sample (Fig. 10). The mismatch is significant if we consider the red model lines (model stars selected by their synthetic FUV-NUV color), which should be the most consistent with the observed sample selection, to the extent that the model atmospheres used by TRILEGAL are correct. Therefore, we explored also the case of a Kalirai et al. (2008) IFMR: the predicted counts are lower at faint magnitudes (especially the halo component fainter than NUV∼22), as expected from Fig. 9-left, while still generally in line with the bright star counts. Because of the incompleteness of our sample at magnitudes fainter than ∼21, and other factors that cannot be conclusively constrained with the current sample, we defer more quantitative conclusions which rests on a comparison of faint stars to a future work, and we adopt in this work the W2000 IFMR, that matches well the bright star counts, to explore other effects.

4.3 Milky Way geometry

As explained above, the default parameters, in particular the MW geometry, in the TRILEGAL code were defined from previous applications of this code to analysis of stellar counts from several surveys. Particularly important in this context were the 2MASS star counts, which are sensi-

tive to the low-mass stars ($<0.8 M_\odot$). These low-mass stars do not overlap with the mass range of the hot-WD progenitors (about 0.8-$8 M_\odot$), however they are very numerous and long-lived, and are little affected by uncertainties in stellar evolutionary models. Therefore we should expect the geometry to be well constrained by previous works, except for the limited extent of the previous surveys.

The agreement between our data and model predictions (with W2000 IFMR) is generally good at bright magnitudes, where our sample is complete. In more detail, we should also explore the dependence of observed and predicted stellar counts with longitude. The effect is more prominent towards the Galactic plane, therefore we examined latitudes between 20-$30°$ North and South, and computed models with evenly spaced coverage along these strips. The models predict, as expected, different counts towards the Galaxy center and anti-center, shown in Fig. 11. The coverage of our present GALEX-SDSS matched catalog at low latitudes is still too sparse for a conclusive comparison, which will be instead attempted by matching the AIS data with GSC2, and with the increased MIS coverage expected in the GALEX "Extended Mission" phase.

Finally, because our UV-optical matched samples are complete to UV magnitudes brighter than $\sim$20-21, therefore mostly sensitive to the thin disk population (Fig.s 8 and 10), and because the models with default MW geometry slightly overpredict the stellar counts at low (especially Northern) Galactic latitudes, we explored different geometries of the thin disk with TRILEGAL. In particular, in Fig. 12 we show the effect of adopting more strongly peaked density distributions at the Galactic Plane: either the simple vertical exponential law, $\propto \rho^{z/h_z}$ (which has been adopted in many MW models, starting from the classical Bahcall & Soneira (1980, 1984)'s), or the simple hyperbolic secant law, $\mathrm{sech}(2z/h_z)$. The results confirm that the default geometry adopted by Girardi et al. (2005) and in this work, i.e. the squared hyperbolic secant law, provide the closest prediction to the observed counts. The same distribution does also provide a good match to star counts of "normal stars" in 2MASS and in the local Hipparcos sample (Girardi et al. 2005). The slight overprediction and underprediction of hot star counts at certain latitudes may also be due to extinction by interstellar dust, which may be either patchy (as in fact it is) or have a slightly different distribution than assumed. These remaining discrepancies and the effects of dust distribution may be addressed with a wider MIS coverage in the future.

4.4 The kinematic of Milky Way stars

The plots of stellar density versus Galactic latitude presented in the previous Sections clearly indicate that we are looking at a population of objects for which the mean distance is larger than the mean scale height on the thin disk. At typical distances of a few hundred parsecs, there will be no parallax measurements for such stars. The most direct distance information we can find for them is related to their proper motions.

The table "USNO" in the SDSS database contains proper motions for SDSS objects made after recalibrating USNO-B1.0 (Munn et al. (2004)) against SDSS astrometry. The systematic errors are quoted to less than 1 mas/year.

The UCAC3 proper motion catalog is strongly incomplete for our sample, owing to its magnitude limit of $f.mag \sim 17$ (which roughly corresponds to $r \sim 17$). In fact, we checked and found that just a handful of our hot-WD candidates is present in UCAC3.

Figure 13 presents the histograms of proper motions, μ, for the hot stars in the 20-30N strip of MIS, and for three different cuts in NUV magnitude. The observed distributions are compared with those predicted from the TRILEGAL models, computed for the same area and for the W2000 IFMR. The model distributions are derived as follows. The observed velocity ellipsoids ($\sigma_U, \sigma_V, \sigma_W$) of each Galaxy component are taken form the literature. Each simulated star is then given a random space velocity that follows the Schwarzschild distribution for this ellipsoid. Space velocities are then corrected for the solar motion (cf. Dehnen & Binney 1998) and projected on the sky using the transformations derived from Hipparcos. The final results are simulated proper motions and radial velocities. We adopt an age-dependent velocity ellipsoid for the thin disk, derived from the Geneva-Copenhagen Survey of Solar neighbourhood (Holmberg et al. 2008). For the thick disk and halo, velocity ellipsoids are taken from Layden et al. (1996). These prescriptions provide a first-order description of the general distributions of proper motions and radial velocities, but are not expected to describe the details of the local velocity streams, nor the effects caused by disk shear in the more distant stars. Moreover, we do not simulate measurement errors in the proper motions. More details will be given elsewhere.

The upper panel of figure 13-right compares the observed and model distributions for a bright WD sample, with a cut at NUV<18mag. There is quite good agreement both in the numbers and distributions of proper motions. The agreement in the numbers derives from the fact that the photometry is quite complete, and just 4% of this bright subsample does not have a proper motion listed in USNO-B. This means that both photometry and proper motion information are very complete in this case, and quite similar to the ones expected for a thin disk population.

The middle and bottom panels of Fig. 13-right compare the observed and simulated μ distribution for fainter samples, with cuts at NUV<19.5 and NUV<21.5mag, respectively. It shows that these samples become incomplete, first in the proper motions at NUV=19.5, and then in photometry at magnitudes NUV=21.5. Note for instance the increasing fraction of stars without proper motion measurement in USNO-B, which goes from 13 to 54% from NUV<19.5 to NUV<21.5.

From this comparison we conclude that our hot WDs do follow the kinematics expected for the thin disk, even if the proper motion information is severely incomplete for the faintest WD candidates.

Distance distributions predicted by the same models are shown in Fig. 13-left. This plot indicates that the brigtest (and complete) MIS sample of NUV<18mag is likely made of WDs located in the thin disk at typical distances between 0.15 and 1 kpc in the latitude range 20-30° North. The fainter sample could instead contain a significant fraction of stars at distances larger than 2 kpc, comprising also a small fraction of thick disk and halo WDs. Note however that this distribution of distances is inferred from models, and we presently have no data to verify the distances of our
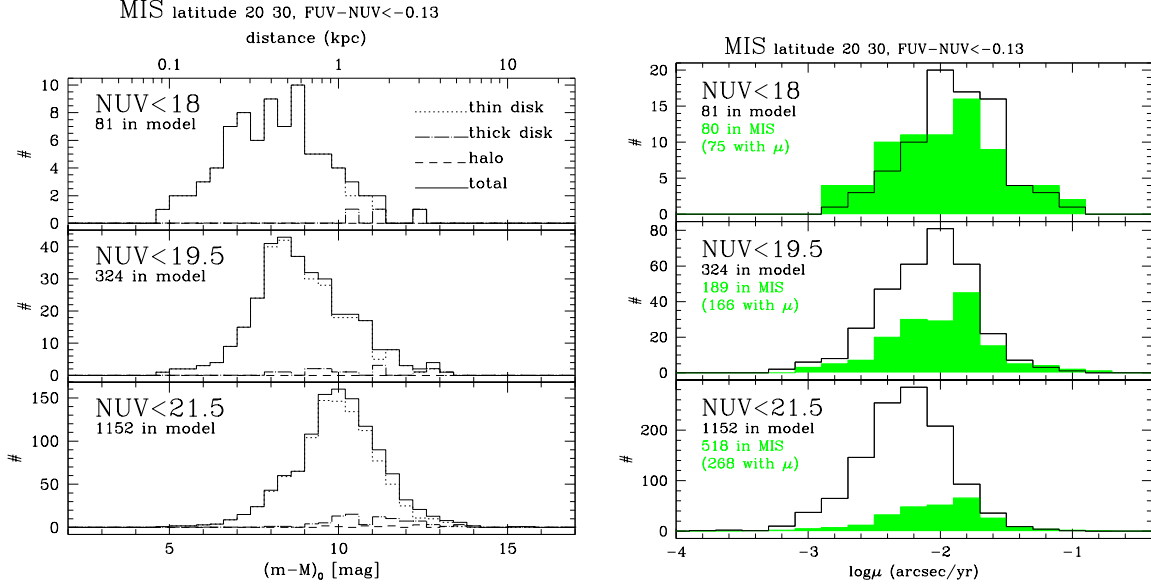
Figure 13. Left: Distance distributions predicted by our TRILEGAL models for the hot stars in the 20-30N strip of MIS, and for three different cuts in NUV magnitude. This plot indicates that the brightest (and complete) MIS sample of NUV<18mag is likely made of WDs located in the thin disk at typical distances between 0.15 and 1 kpc (in this latitude range). The faintest samples could instead contain a significant fraction of stars at distances larger than 2 kpc, comprising also a small fraction of thick disk and halo WDs. Right: distribution of proper motions (amplitudes): observed distribution (green solid histograms) are compared to model predictions (continuous lines), computed for the same area. The numbers in each panel indicate the NUV magnitude cut, the number of predicted hot stars, of observed ones in MIS, and of those which have proper motion information from USNO-B.
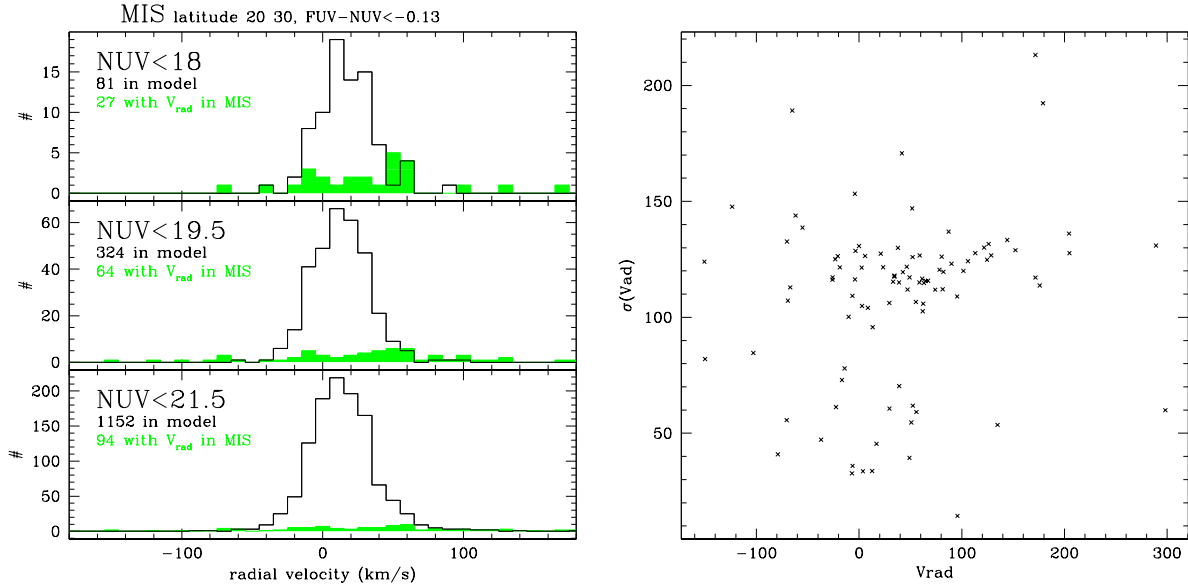
Figure 14. Distribution of velocities (left) from the SDSS spectroscopic pipeline for the subsample of MIS hot stars with spectra. The comparison is inconclusive because of the large errors (often larger than the values) in the pipeline velocity measurements, shown in the right panel.

sample stars, but for the proper motions already depicted in Fig. 13 (right); future work will address identification of thick disk and halo objects with follow-up spectroscopy. The distance distribution is fairly similar at other latitudes.

Finally, Fig.14 presents the expected distributions of

radial velocities for the latitude 20-30N sample, from the models, and the radial velocities derived from SDSS spectra, available for a subsample of our hot star catalog (section 3.2). This is a biased subset because the choice of SDSS spectroscopic targets is obviously unrelated to our selection

of hot stellar objects. The worse effect however, making the comparison inconclusive, is the large errors in velocity determinations from the SDSS pipeline (see Fig. 14-right).

5   CONCLUSIONS AND SUMMARY

From GALEX's data release GR5 we constructed catalogs of unique UV sources (i.e. eliminating repeated observations), and subcatalogs with matched SDSS optical photometry. We extracted catalogs of hot star candidates (FUV-NUV<-0.13), mostly comprised of hot WDs. Over 38,000 such sources with photometric error $\leqslant 0.3$mag, have SDSS photometry ($\sim$74,000 with UV photometric error $\leqslant 0.5$mag), excluding UV sources with multiple optical matches, that are between $\sim$8 to 30% of the total. The GALEX surveys AIS and MIS cover different latitudes at their respective depths ($\sim$21 and $\sim$23 AB mag), enabling a first quantitative analysis of the hot-WD stellar population with Milky Way models. Current descriptions of MW stellar components (halo, thin and thick disk) are mostly based on stellar counts of low mass ($<0.8M_\odot$) stars (2MASS, shallow but all-sky, plus a few deep but area-limited surveys). We explored in this work different thin disk geometries and different IFMR. GALEX provides an unprecedented census of the evolved descendants of 0.8-8$M_\odot$ stars, and the analysis of our current hot-WD sample places some constraints on the initial-final mass relation (IFMR), one of the crucial ingredients to understand the chemical enrichment of the ISM.

The brightest (and complete) sample is likely made of hot WDs located in the thin disk at typical distances between 0.15 and 1 kpc. The faintest samples could instead contain a significant fraction of stars at distances larger than 2 kpc, comprising also hot WDs in the thick disk and halo. This work is based on the analysis of matched GALEX-SDSS sources, and the SDSS magnitude limit prevents analysis of thick-disk and halo components. Hot WDs are however detectable at such larger distances at MIS depth (see dark-green histograms in Fig.s 8 and 10, and section 3.1), and will be investigated in a future work with deeper optical data.

Model predictions of hot star counts at different latitudes, computed with currently accepted MW geometry, and assuming W2000 IFMR, match the data quite well at intermediate latitudes and bright magnitudes, but are somewhat discrepant at low latitudes and faint magnitudes. There is a slight but systematic North-South asymmetry, and MW models with canonical geometry for stars and dust match better the data at Southern low latitudes, and at Northern high latitudes, indicating that the dust distribution on the MW disk may also be better constrained by our data than was previously possible. The dust distribution will be investigated with the future more extended sky coverage from the ongoing GALEX mission. However, the observed asymmetry may also be due to the longitude dependence of the stellar populations, as our present matched-sources sample covers unevenly North and South Galactic latitudes (Fig. 1). Our MIS matched-sources sample is incomplete at magnitudes fainter than about $\sim$21.5 due to the SDSS limits for the hottest sources. At all latitudes, and at magnitudes where the samples are complete, MW model predictions of hot WD counts computed with IFMRs favouring lower final masses match the GALEX hot WD counts significantly better than

the IFMR currently postulated by Marigo & Girardi (2007) from AGB stars data. This result contributes an important constraint to stellar evolution in the final phases which drive the yield of chemical elements.

5.1   The implications for stellar evolution

What are the implications of constraining the IFMR for the galaxy chemical evolution? The IFMR contains the record of the nucleosynthesis history during the TP-AGB phase, as well as determines the contribution of AGB stars in terms of dark remnants. The IFMR, and the final yield of chemical elements, are significantly affected by the occurrence (or not) of the so-called "third dredge-up". At each dredge-up episode the core mass is reduced by an amount $\Delta M_{\rm dredge} = \lambda\,\Delta M_{\rm c,\,TP}$, where λ is the classical efficiency parameter, and $\Delta M_{\rm c,\,TP}$ denotes the mass growth of the core during the preceeding interpulse period.

In the extreme case where $\lambda \sim 1$, no increment of the C-O core is predicted. As a consequence, for low-mass stars not experiencing the third dredge-up ($\lambda = 0$, $M < M_{\rm min}^{\rm dredge}$), the remnant mass scales directly with the duration of the TP-AGB lifetime, while for stars in which the third dredge-up takes place ($\lambda > 0$, $M \geqslant M_{\rm min}^{\rm dredge}$) this simple proportionality is replaced by a more complex interplay between core growth, dredge-up, and mass loss. For such more massive stars ($M \geqslant M_{\rm min}^{\rm dredge}$, where $M_{\rm min}^{\rm dredge} \approx 1.0 - 1.5\ M_\odot$, depending on metallicity and model details) the final mass and the chemical yields are related as we will briefly discuss below (see Marigo & Girardi 2001 for more details).

For the generic element k, the corresponding AGB yield is defined as:

$$M_y^{\rm AGB}(k) = \int_{\tau_{\rm AGB}} [X_k(t) - X_k^0]\dot{M}(t)\,dt \qquad (5)$$

where X_i^0 is the initial abundance at the epoch of star formation, $X_i(t)$ is the value at time t, and $\dot{M}(t)$ is the current mass-loss rate.

Let us first consider, in the IFMRs in Fig. 9, the part for $M_{\rm ini} < M_{\rm min}^{\rm dredge}$. The chemical yields produced by these stars (mainly ^{13}C, ^{14}N, and ^{4}He) are determined by the first dredge-up, and the cool-bottom process (Boothroyd & Sackmann 1999) or thermohaline mixing (Charbonnel & Zahn 2007) operating during the RGB, as no subsequent dredge-up events take place on the AGB according to the standard stellar evolution theory. For these low-mass stars the AGB yield, defined by Eq. (5), simplifies as $M_y^{\rm AGB}(k) = [X_k^{\rm RGB} - X_k^0]\Delta M_{\rm AGB}^{\rm ej}$, where $X_k^{\rm RGB}$ is the surface abundance left after the RGB phase, and $\Delta M_{\rm AGB}^{\rm ej}$ is the total amount of mass ejected on the AGB. In turn, the expelled mass is related to the final mass through $\Delta M_{\rm AGB}^{\rm ej} = M_{\rm AGB,0} - M_{\rm final}$, where $M_{\rm AGB,0}$ denotes the stellar mass at the onset of the AGB phase. The final masses of these stars with $M_{\rm ini} < M_{\rm min}^{\rm dredge}$ can be reduced by simply invoking more efficient mass-loss along the AGB. Their chemical yields would increase correspondingly, since less envelope mass will be locked in the central core following the outward displacement of the H-burning shell, so that $\Delta M_{\rm AGB}^{\rm ej}$ will be larger. For instance, for an AGB mass of $M_{\rm AGB,0} = 1.2\ M_\odot$, a final mass $M_{\rm final} = 0.55\ M_\odot$ versus $M_{\rm final} = 0.60\ M_\odot$ would imply an increase of the AGB

chemical yield by $(0.60 - 0.55)/(1.2 - 0.60) \approx 10\%$, as well as a larger total chemical yield, including the RGB wind contribution.

For $M_{\mathrm{initial}} \geqslant M_{\min}^{\mathrm{dredge}}$, in addition to the first dredge-up (and possibly second dredge-up on the Early-AGB), the chemical yields include also the enrichment, mainly in ^{4}He and primary ^{12}C, produced by the He-shell flashes and brought up to the surface by the third dredge-up, and the enrichment of ^{14}N produced by the hot-bottom burning process occurring in the most massive AGB stars ($M_{\mathrm{initial}} \gtrsim 4.0 - 4.5\ M_\odot$). Again smaller final masses are reached when higher mass-loss rates occur, and/or deeper dredge-up (i.e. larger λ). These two factors may affect the chemical yields in opposite ways. On one hand, a high mass loss limits the number of dredge-up episodes, hence lowering the chemical yields; on the other hand, a deeper dredge-up conveys larger amounts of carbon and helium to the surface layer, which are then ejected. In addition, mass loss and dredge-up efficiency are actually inter-related, a larger surface C abundance generally favouring stronger dust-driven mass loss in C stars (e.g. Mattsson et al. 2008), while a significant reduction of the mass of the envelope may decrease its penetration (i.e. lower λ) during the third dredge-up (see, e.g. Karakas et al. 2002). In sum, a higher mass expelled does not directly imply that such material is relatively more enriched of processed elements.

An IFMR similar to Weidemann (2000) weighs the final masses towards lower values than e.g. the IFRM of MG07 in the range $M_{\mathrm{initial}} \lesssim 3.0 M_\odot$, while the two relations essentially agree at higher M_{initial}. For $M_{\mathrm{initial}} \lesssim M_{\min}^{\mathrm{dredge}}$, forcing the theoretical IFMR to converge on a W2000-type IFMR by assuming a higher mass loss would produce a modest increase of the chemical yields from these objects (because more mass is ejected), compared to the MG07 IMFR case. As for the initial mass range $M_{\min}^{\mathrm{dredge}} \leqslant M_{\mathrm{initial}} \leqslant 3.0\ M_\odot$, a higher mass loss (necessary to reach a smaller final mass, as suggested by our WD counts) may reduce the number of dredge-up episodes on the TP-AGB and this may lead to a lower yield of processed material. In other words, constraining the IFMR translates into constraining the total mass lost in the AGB phase. The chemical composition of the ejecta from these stars, however, is also critically sensitive to the depth of the third dredge-up, which can be calibrated by measurements of abundances in Planetary Nebulae (Marigo et al 2003) and by a better estimate of the duration of the AGB phase at different metallicity (Marigo et al. in prep.).

5.2   Future Work

With the current MIS coverage (1,103 square degrees overlapping with SDSS photometry in GR5), we compared with MW models stellar counts summed in $10°$ latitude strips, combining all longitudes in order to obtain acceptable statistics. In order to disentangle geometry of the stellar populations, dust extinction, and stellar evolution in more detail, we need to analyze also the longitude dependence of stellar counts, as demonstrated by Fig.s 10 and 11. We will explore dust effects in the MW disk by matching the AIS with GSC2, for a larger sky coverage (see Bianchi et al (2011)). The density of hot stars (the rarest in nature) is very low and large area coverage is needed for good statistics.

The MW halo and thick disk components, however, become significant at UV magnitudes fainter than about 21, therefore require a wider MIS coverage (planned in the GALEX Extended Mission phase) to be usefully constrained (see fig.s 1, 8 and 10), and deeper optical surveys.

Finally, hot-WDs in binaries, again elusive at optical wavelengths, are uniquely and unambiguously revealed and characterized by the GALEX UV sky survey, matched to optical surveys. These binaries sample different types of stellar pairs (different T_{eff} ranges) than those detected and characterized by optical surveys, thanks to the UV photometry (e.g. Fig.6 of Bianchi et al. (2007b)). Because our current photometric selection includes contamination by extragalactic objects in the "binary" *locus*, and on the other hand the binaries do not significantly change the distribution of stellar counts, which was the subject of the present analysis, the binary candidates will be investigated in a future work.

5.3   Final remarks. The online catalogs.

The present catalog of "single" hot star candidates has a high purity, as estimated from the serendipitous (but not unbiased) spectroscopic SDSS coverage. While we expect most of the hottest sources to be high gravity objects (CSPN, subdwarfs or WD), we did not apply any cut in gravity, therefore main sequence stars and supergiants hotter than $\sim$18,000K are also included in our catalogs. Their number is very small compared to the evolved stars, however their inclusion in the catalog makes it more generally useful.

Finally, we remind future users of our catalogs that GALEX UV sources with more than one optical counterpart were excluded from the analysis of the hot-star sample, (and should be excluded from any sample based on photometric color selection), but their fraction can be corrected statistically using Table 2. They are included (flagged with "rank"=1) in our online catalogs. A few percent of the matched sources may be spurious matches (Fig. 3) but these would mostly have random UV-optical colors. The hot-star candidates with NUV-r>0.1, includes also some extragalactic objects, the relative fraction is magnitude and latitude dependent.

The source catalogs (GALEX unique sources, GALEX-SDSS matched sources, hot-stars samples) are available in electronic form only, from the author's web site (http://dolomiti.pha.jhu.edu/uvsky) where files description can be found, and will be also posted on MAST (http://galex.stsci.edu and http://archive.stsci.edu/hlsp/). A statistical analysis and discussion of properties, useful to potential users of our (and similar) catalogs for understanding completeness and biases of any sample selection is given by Bianchi et al (2011).

REFERENCES

Althaus, L. G., García-Berro, E., Isern, J., & Córsico, A. H. 2005, A.A., 441, 689

Althaus, L. G., Serenelli, A. M., & Benvenuto, O. G. 2001, MNRAS, 323, 471

Bahcall, J. N., & Soneira, R. M. 1980, ApJs, 44, 73

—. 1984, ApJs, 55, 67

Bergeron, P., Ruiz, M. T., & Leggett, S. K. 1997, ApJs, 108, 339

Bergeron, P., Saffer, R. A., & Liebert, J. 1992, ApJ, 394, 228

Bianchi, L. 2011, APSS, in press (special issue "UV Universe 2010", editors B. Shustov, A.I. Gomez de Castro, and M. Sachkov)

Bianchi, L. 2009, APSS, 320, 11

Bianchi, L., Herald, J., Efremova, B, et al 2011, APSS, in press (special issue "UV Universe 2010", editors B. Shustov, A.I. Gomez de Castro, and M. Sachkov)

Bianchi, L., Hutchings, J.B., Efremova, B. et al. 2009a, AJ, 137, 3761

Bianchi, L., Efremova, B., Herald, J. et al. 2009b, in "Future Directions in Ultraviolet Spectroscopy", eds.Van Steenberg et al AIPC, 1135, 326

Bianchi, L. 2007, in UV Astronomy: Stars from Birth to Death, eds. A. Gomez de Castro & M. Barstow, ISBN 978-84-7491-852-6, p. 65

Bianchi, L., et al. 2007a, ApJS, 173, 659

Bianchi, L., et al. 2007b, in "UV Astronomy: Stars from Birth to Death", ed. A. Gomez de Castro & M. Barstow, ISBN 978-84-7491-852-6, p.95

Bianchi, L., et al. 2005, ApJ, 619, L27

Bianchi, L., Madore, B., Thilker, D., Gil de Paz, A., Martin, C., & The GALEX Team 2003, in "The Local Group as an Astrophysical Laboratory", STScI publ., M.Livio and T.Brown eds., p.10

Boothroyd A. I., Sackmann I.-J., 1999, ApJ, 510, 232

Bragaglia, A., Renzini, A., & Bergeron, P. 1995, ApJ, 443, 735

Budavari, T., et al. 2009, ApJ, 694, 1281

Charbonnel C., Zahn J.-P., 2007, A&A, 467, L15

Croom et al. 2004, MNRAS, 349, 1397

Dehnen, W. & Binney, J.J. 1998, MNRAS, 298, 387

de Martino, C., Bianchi, L., Pagano, I., Herald, J., Thilker, D. 2008, Mem.SAIt, eds. S. Cassisi & M. Salaris, Vol. 79, p. 704 (2008) (arXiv:0712.0755)

Dupuis, J. 2002, ASP Conf.Series, 264, 15

Eisenstein, D.J., et al. 2006, ApJS, 167, 40

Ferrario, L., Wickramasinghe, D., Liebert, J., & Williams, K. A. 2005, MNRAS, 361, 1131

Fleming, T.A., et al. 1996, A&A, 316, 147

Gaeensike, B.T., et al 2009, MNRAS, 397, 2170

Gil de Paz, A. et al. 2007, ApJS, 173, 185

Girardi, L., Groenewegen, M. A. T.,Hatziminaoglou, E., & da Costa, L. 2005, A.A., 436, 895

Gontcharov, G.A. et al 2010, astro-ph 1003.3456

Hansen, B. M. S., & Liebert, J. 2003, ARAA, 41, 465

Harris, H.C., et al. 2008, ApJ 679, 697

Heller, R., Homeier, D., Dreizler, S. 2009, A&A, 496, 191

Holberg, J. B.,Oswalt, T., Sion, E. M. 2002, ApJ, 571, 512

Holberg, J. B., Sion, E. M., Oswalt, T., McCook, G. P., Foran, S., & Subasavage, J. P. 2008, AJ, 135, 1225

Holmberg, J., Nordström, B., & Andersen, J. 2009, A.A., 501, 941

Hu, Q., Wu, C., & Wu, X. 2007, A.A., 466, 627

Kalirai, J. S., Hansen, B. M. S., Kelson, D. D., Reitzel, D. B., Rich, R. M., & Richer, H. B. 2008, ApJ, 676, 594

Kalirai, J. S., Saul Davis, D., Richer, H. B., Bergeron, P., Catelan, M., Hansen, B. M. S., & Rich, R. M. 2009, ApJ, 705, 408

Karakas A. I., 2010, MNRAS, 403, 1413

Karakas, A. I.; Lattanzio, J. C.; Pols, O. R. 2002, Publications of the Astronomical Society of Australia, Volume 19, Issue 4, p. 515

Kepler, S. O., Kleinman, S. J., Nitta, A., Koester, D., Castanheira, B. G., Giovannini, O., Costa, A. F. M., & Althaus, L. 2007, MNRAS, 375, 1315

Kleinman, S.J, Nitta, A., & Koester, D. 2009, Journal of Physics: Conference Series, Volume 172, Issue 1, p. 2020

Koester, D. 2008, Mem. SAIt. Vo.75, 282

Layden, A.C. et al. 1996, AJ, 112, 2110

Liebert, J., Bergeron, P., & Holberg, J. B. 2005, ApJs, 156, 47

Madej, J., Należyty, M., & Althaus, L. G. 2004, A.A., 419, L5

Marigo, P. 2001, A.A., 370, 194

Marigo P., Bernard Salas J., Pottasch S. R., Tielens A. G. G. M., Wesselius P. R., 2003, A.A., 409, 619

Marigo P., Girardi L., 2001, A&A, 377, 132

Marigo, P., & Girardi, L. 2007, A.A., 469, 239

Mattsson, L., Wahlin, R., Höfner, S., & Eriksson, K. 2008, A.A., 484, L5

Mc Cook, G.P. & Sion, E.M. 1999, ApJS, 121, 1

Morrissey, P., et al. 2007, ApJS, 173, 682

Munn, J. A., et al. 2004, AJ, 127, 3034

Rebassa-Mansergas, A., et al. 2010, MNRAS, 402, 620

Rocha-Pinto, H. J., Maciel, W. J., Scalo, J., & Flynn, C. 2000, A.A., 358, 850

Salpeter, E. E. 1955, ApJ, 121, 161

Schlegel, D. J., Finkbeiner, D. P., & Davis, M. 1998, ApJ, 500, 525

Silvestri, N.M. et al 2007, AJ, 134, 741

Szkody, P. et al. 2009, AJ, 137, 4011

Tremblay & Bergeron, 2007, ApJ 657, 1013

Vassiliadis, E., & Wood, P. R. 1994, ApJs, 92, 125

Vennes, S. et al 2002, MNRAS, 335, 673

Watcher, S., Hoard, D.W., Hansen, K.H. et al. 2003, ApJ, 586, 1356

Weidemann, V. 2000, A.A., 363, 647

Table 1. Sky coverage for GR5 MIS and AIS, and GR5xDR7

Latitude range	—— area [deg^2] ——		E(B-V)^a	
	GALEX GR5	GR5+DR7	mean	1σ
MIS				
-90 -80	29.4	0.0	n.a.	n.a.
-80 -70	59.3	19.3	0.04	0.01
-70 -60	257.4	99.2	0.03	0.01
-60 -50	242.5	86.2	0.05	0.02
-50 -40	150.5	120.4	0.06	0.02
-40 -30	109.0	68.04	0.07	0.03
-30 -20	27.4	25.5	0.08	0.02
-20 -10	0.0	0.0	n.a.	n.a.
-10 0	0.0	0.0	n.a.	n.a.
0 10	0.0	0.0	n.a.	n.a.
10 20	5.8	5.0	0.04	0.01
20 30	89.1	85.5	0.04	0.01
30 40	210.3	203.2	0.04	0.02
40 50	161.3	157.1	0.03	0.02
50 60	175.7	173.0	0.04	0.01
60 70	58.1	58.1	0.03	0.01
70 80	2.8	2.8	0.02	0.00
80 90	0.0	0.0	n.a.	n.a.
Total:	1578.6	1103.0	0.04	0.02
AIS				
-90 -80	249.3	0.0	0.02	0.00
-80 -70	714.0	99.6	0.03	0.01
-70 -60	1137.4	128.4	0.03	0.01
-60 -50	1490.2	223.4	0.05	0.02
-50 -40	1752.0	306.8	0.07	0.03
-40 -30	1910.2	268.8	0.09	0.06
-30 -20	1616.3	168.7	0.10	0.06
-20 -10	1015.9	100.9	0.17	0.10
-10 0	211.3	37.6	0.41	0.24
0 10	349.5	27.4	0.45	0.31
10 20	1487.0	156.3	0.12	0.14
20 30	2002.1	454.5	0.06	0.05
30 40	2115.2	917.9	0.05	0.02
40 50	1866.2	1174.7	0.03	0.02
50 60	1480.0	1221.2	0.03	0.01
60 70	1067.3	1067.3	0.02	0.01
70 80	738.0	738.0	0.02	0.01
80 90	233.2	233.2	0.02	0.01
Total:	21434.8	7324.5	0.05	0.07

(a) E_{B-V} values are computed from the Schlegel et al. (1998) maps for the centers of the GALEX fields, then averaged. They do not reflect an average Galactic trend, since they follow the specific distribution of fields shown in Fig. 1, which is rather non uniform at low latitudes

Table 2. Statistical characteristics of the Catalogs and effects of error cuts

Latitude range		# GALEX sources $err_{NUV} \leqslant 0.5$	# GALEX sources $err_{FUV,NUV} \leqslant 0.5$	# GALEX sources FUV-NUV<-0.13 $err_{FUV,NUV} \leqslant 0.5$	$err_{FUV,NUV} \leqslant 0.3$	# matched sources $err_{NUV} \leqslant 0.5$ rank0	rank1	$err_{NUV,FUV} \leqslant 0.5$ rank0	rank1	$err_{NUV,FUV} \leqslant 0.3$ rank0	rank1	# Pointlike matched $err_{NUV} \leqslant 0.5$ rank0	rank1	$err_{NUV,FUV} \leqslant 0.5$ rank0	rank1	$err_{NUV,FUV} \leqslant 0.3$ rank0	rank1	with FUV-NUV<-0.13 $err_{NUV,FUV} \leqslant 0.5$	$\leqslant 0.3$	NUV-r<0.1 $\leqslant 0.3$
MIS																				
-90	-85	66929	16822	2444	622	0	0	0	0	0	0	0	0	0	0	0	0	0	0	0
-85	-80	177553	49043	6304	1540	0	0	0	0	0	0	0	0	0	0	0	0	0	0	0
-80	-75	112394	32092	4021	971	0	0	0	0	0	0	0	0	0	0	0	0	0	0	0
-75	-70	394332	109647	12984	3070	87456	2708	33147	1300	15510	794	17782	638	2584	211	1158	127	321	91	42
-70	-65	798670	223254	25020	6151	156597	3994	63005	2099	34584	1450	33311	1021	5554	345	2759	224	671	201	78
-65	-60	1409943	400165	44106	11391	360403	10991	149854	5826	87609	4079	71801	2433	12151	866	6395	565	1386	426	155
-60	-55	1244707	328909	40804	10773	228705	7106	86721	3448	49148	2388	49844	1659	7401	501	4061	334	931	296	125
-55	-50	632803	143121	21932	6162	164257	5294	49621	2093	25136	1291	41518	1388	4477	308	2374	204	711	257	112
-50	-45	609861	137541	21637	5756	304497	12522	92372	5102	46024	3217	77719	3427	8067	812	4342	506	1230	472	244
-45	-40	428767	89077	13169	3620	207041	10578	57421	3948	29654	2414	61074	3127	5178	651	2869	413	745	311	157
-40	-35	538838	103347	15242	4283	211133	9835	50373	3174	27961	1978	83015	3652	6030	580	3634	349	843	396	228
-35	-30	323258	59584	8370	2715	124660	8736	27139	2794	16141	1929	58244	3735	3658	607	2374	419	558	303	174
-30	-25	214275	31837	5398	1749	133209	8714	23127	2116	11900	1213	75788	4697	4076	529	2404	301	656	365	240
-25	-20	48433	6190	1035	357	34035	2638	4825	494	2441	272	22202	1652	1109	149	646	94	182	93	65
15	20	43887	8626	997	304	26939	1383	6195	433	3488	279	14452	716	1297	120	812	81	132	77	51
20	25	226867	47323	6099	1672	144508	7255	35983	2484	18325	1450	64767	3040	5810	575	3372	358	635	308	218
25	30	403868	91523	10958	2782	281365	12461	79869	4695	39329	2745	101054	4591	10017	974	5594	565	1075	520	346
30	35	711824	152925	21310	5682	474446	18387	132915	6920	66709	4116	155923	6218	14995	1263	8182	727	2079	862	488
35	40	937945	203696	27963	7589	621803	24188	173805	9065	91210	5604	200400	8114	18511	1602	10080	971	2720	1094	601
40	45	641846	152205	21044	5661	430026	15963	133123	6575	68076	4018	119976	4803	12413	1116	6306	654	1892	744	413
45	50	707063	162317	21478	5659	460636	15730	139985	6496	74669	4238	127343	4598	12844	1041	6839	658	1885	639	325
50	55	731762	170967	20334	5143	492531	19798	149059	7947	80742	4944	135058	5360	13351	1257	7468	769	1700	641	371
55	60	690921	170036	20115	4864	461420	18063	146692	7491	76642	4663	119973	4788	12470	1150	6521	704	1657	528	293
60	65	377644	97916	11366	2899	255057	9001	86150	4034	45134	2581	62828	2388	7169	649	3695	415	912	309	142
65	70	99569	25651	3073	716	68009	2407	22683	1058	10337	609	13951	546	1857	151	832	83	238	75	44
70	75	23953	6405	678	136	16778	537	5757	238	2588	137	3126	137	446	46	198	26	62	20	12
-90	90	12597912	3020219	387881	102267	5745511	228289	1749821	89830	923357	56409	1711149	72728	171465	15503	92915	9547	23221	9028	4924
AIS																				
-85	-90	186959	29800	6088	1187	2118	66	488	22	137	9	686	24	60	2	21	1	5	0	0
-80	-85	639403	107385	20863	4235	15996	448	3458	144	1075	65	4635	152	399	33	177	17	55	28	24
-75	-80	946695	157960	31268	6157	42060	1425	9492	431	2998	179	11306	416	922	79	448	32	134	60	41
-70	-75	1379695	220313	43504	8513	102750	4001	23114	1254	7740	600	28113	1238	2273	223	1058	116	309	138	97
-65	-70	1779025	267234	53565	10329	104406	3670	24373	1188	8059	514	28907	1114	2464	221	1070	102	350	141	99
-60	-65	1823298	273723	54203	10650	151592	6068	34985	1981	11556	944	44240	1714	3466	342	1584	181	489	233	176
-55	-60	2202425	309450	62380	12610	149424	6616	29732	1895	9752	819	50822	2148	3580	355	1700	168	537	294	214
-50	-55	2221574	260072	55813	11764	137391	6620	21591	1640	7251	732	56334	2497	3270	348	1589	154	553	331	234
-45	-50	2526007	271544	59711	12805	195821	10880	29085	2665	10396	1253	81131	4309	4433	562	2221	277	801	473	338
-40	-45	2644017	259939	59142	14759	157644	12248	20715	3038	7274	1400	79249	5390	3708	680	1808	341	758	441	302
-35	-40	2824496	243813	55332	13542	243682	15446	28209	3371	9899	1562	133778	7605	5717	831	2900	417	1208	725	501
-30	-35	3022905	251126	53008	14535	171132	14681	14919	2977	5579	1395	112514	7969	4148	857	2175	454	938	570	394
-25	-30	2725467	171367	39306	12449	219113	20491	15759	3593	6299	1665	159944	12263	5423	1154	2978	571	1330	829	611
-20	-25	2565319	121358	29997	11039	158390	19012	7832	2255	3563	1116	133521	13447	4060	922	2233	504	1037	650	476
-15	-20	2294738	90915	21775	9748	104999	13902	4288	1362	2245	739	94135	10745	2685	665	1536	384	660	406	291
-10	-15	1474126	54091	11682	6026	107441	14988	4086	1142	2582	762	102078	12821	3235	736	2048	511	607	350	231
-5	-10	468735	20256	3196	1719	15893	2690	834	224	547	147	15334	2358	707	158	441	102	77	39	
0	-5	81792	5544	338	126	0	0	0	0	0	0	0	0	0	0	0	0	0	0	0
5	0	112359	9822	673	324	4730	816	364	140	263	120	4577	774	340	133	241	113	37	18	
10	5	896414	41563	5055	2532	67009	10668	4191	1170	2914	871	64784	9577	3683	921	2520	682	285	169	
15	10	2209741	93883	17027	7825	133415	20698	6792	1979	4160	1267	124034	17107	5085	1207	3230	806	758	458	301
20	15	2785094	137819	28011	10512	248149	22946	22199	3385	9760	1708	192683	16088	8372	1376	4610	747	1398	892	688
25	20	3078141	180485	38516	11924	482621	34646	50125	5965	19504	2777	328234	21367	14284	2013	7510	1020	2539	1604	1230
30	25	3074765	199400	45162	11949	565885	34039	59037	6033	20866	2622	336893	18763	14374	1854	7217	885	2777	1683	1308
35	30	3068226	221555	50831	11949	770294	40366	91294	7455	30887	3131	420587	20138	18413	1879	9082	840	3615	2135	1711
40	35	2827184	215451	50937	10501	911569	43682	109497	8095	35498	3333	459207	20279	19905	1846	9697	822	3899	2278	1774
45	40	2867019	241576	57082	10742	1149694	53336	144002	10172	45305	4158	490863	21484	21555	2157	10284	980	4171	2345	1858
50	45	2589087	237387	55351	9692	1187271	53682	158334	10737	47012	4333	455468	19957	21918	2243	10131	1013	4017	2139	1679
55	50	2183650	219294	49511	8631	1135384	51155	165181	11031	48979	4336	414632	18158	21966	2136	9994	973	3845	1979	1556
60	55	2031169	227445	49608	8489	1207517	55161	187254	12923	56759	5317	390611	17457	21534	2264	9850	1071	3576	1838	1497
65	60	1617230	193927	41370	7220	1058375	50788	173459	12127	52661	5039	332166	15743	19066	2203	8630	1048	3063	1531	1197
70	65	1419335	168945	36062	6064	927973	42934	151376	10316	44148	4136	278120	12937	16547	1808	7447	822	2578	1325	1022
75	70	1204662	135513	29867	4605	792486	37015	121558	8221	34147	3190	227147	10912	13190	1494	5749	675	2127	1033	792
80	75	860091	88480	19796	2865	563957	27906	78969	5847	21026	2238	155680	8158	8642	1069	3668	475	1370	645	
85	80	471126	59667	12490	1978	310436	15381	53200	3836	14757	1510	87185	4318	5673	638	2445	290	842	401	307
90	85	164322	20454	4760	795	107786	5417	18269	1330	5094	523	27164	1384	1682	212	754	102	267	138	118
-90	90	65266291	5808556	1253280	290790	13704403	753888	1868061	149944	590692	64510	5926762	340811	286779	35621	139046	17696	51012	28319	21606

Note: The columns "rank0" give the number of UV sources with one SDSS counterpart (within the match radius of $3''$), and "rank1" of those with multiple optical matches.

UV sources with multiple matches may have composite UV colors, therefore are excluded from the analysis sample; their exclusion is accounted for by correcting the density of sources by (rank1/(rank0+rank1)). The fraction from columns 16-17 (from which our analysis sample is extracted) is plotted in Fig. 3. Numbers in columns 18, 19 and 20 include only "rank0" sources.